JUNE 1984 LRP 238/84

LECTURE NOTES

AN INTRODUCTION TO THE THEORY OF ALFVEN WAVE HEATING
(with a side-glance on ICRF)

K. Appert, J. Vaclavik, and L. Villard

LECTURE NOTES

AN INTRODUCTION TO THE THEORY OF ALFVEN WAVE HEATING

(with a side-glance on ICRF)

K. Appert, J. Vaclavik, and L. Villard

These lectures have been presented by K. Appert
at the Universidade Federal Fluminense, Niterói, Brasil
in March/April 1984

CONTENTS

1. INTRODUCTION

This series of lectures is intended to be an introduction to the theory of Alfvén Wave Heating (subsequently AWH). It will largely be based on the studies we have performed in the last few years in Lausanne, and is not meant to be a general review of work in the field. Especially, kinetic aspects of the theory will only briefly be touched upon. For these aspects the reader is referred to the pertinent literature [1,2].

A good deal of the work we have done is numerical. In fact, the mathematical complexity of the problem in real geometries made the numerical treatment a necessity. To us, it seems to be essential to have a good basic knowledge of the underlying physics in Alfvén Wave Heating, especially what concerns the phenomenon of resonant absorption (and linear mode conversion) and the concept of global modes. The computer can do the rest, once these two items are understood.

The frequencies used for Alfvén Wave Heating of present-day devices lie not too far below the ion-cyclotron frequency of the filling gas. They might well lie above the cyclotron frequencies of certain partially stripped impurity ions. The complete theory of Alfvén Wave Heating therefore might imply features of the theory of ICRF heating (ion-cyclotron-range-of-frequency). Moreover, the ion-ion-hybrid mode-conversion scenario of ICRF in the cold plasma model has perfectly the same formal origin as the phenomenon called "Alfvén Wave Heating". We will therefore include a certain number of remarks concerning the ICRF heating scheme.

The classical and most simple problem of absorption of RF energy due to plasma inhomogeneities is the interaction of an electromagnetic wave with the ionosphere [3]. This problem has become topical once more in the seventies in connection with laser-plasma interaction [4].

Let us rapidly review the main features of the 3 mentioned cases of resonant absorption. In the laser case we have a short-wavelength (λ) electromagnetic wave incident onto a plasma whose density increases towards the interior (Fig. 1.1). The characteristic length of the density variation is L.

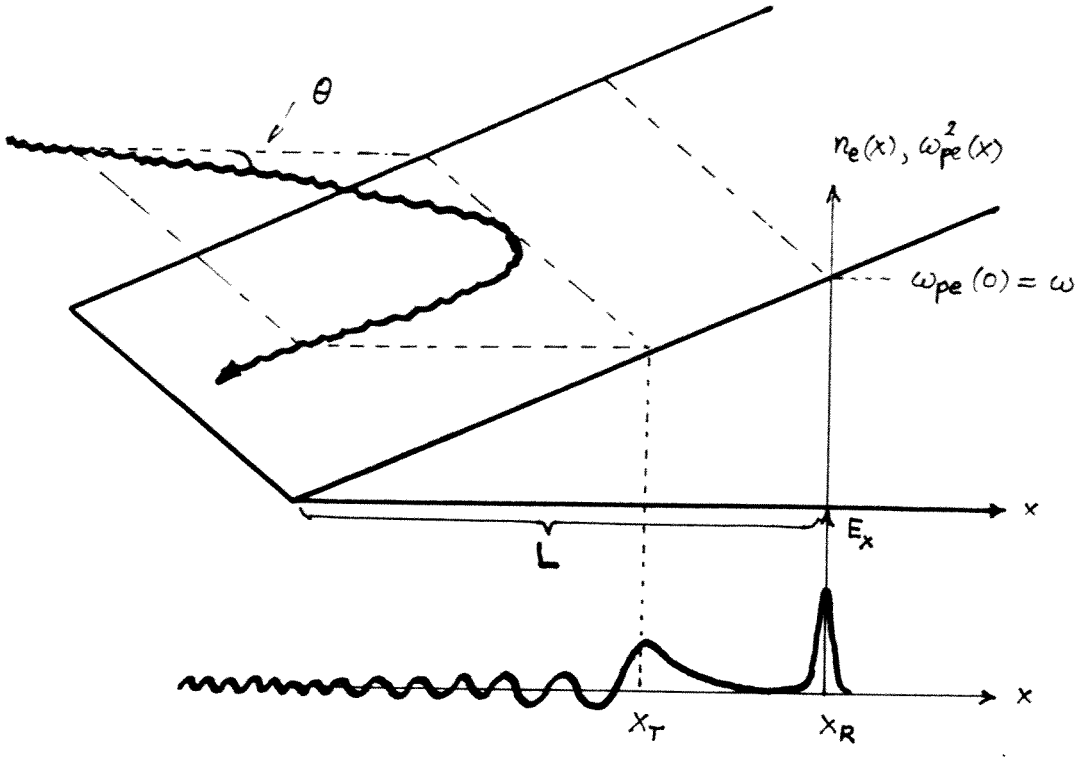

Fig. 1.1

If the incidence is not perfectly perpendicular to the plasma surface the wave is reflected at the turning point x_T before it reaches the "resonance point" x_R, where the wave's frequency matches with the local plasma frequency ω_{pe}. If, however, the angle of incidence is small enough (i.e. x_T near to x_R), some field tunnels through from x_T to x_R where it resonantly excites plasma oscillations. Their amplitude grows in time until either collisions or temperature effects limit the growth. The energy flow from x_T to x_R is independent of these amplitude-limiting effects as long as the collisions are not too frequent nor the temperature too high. In this situation one says that the incoming "energy-carrier" wave has lost energy by resonant absorption.

The resonant point x_R (and x_T as well) can be moved throughout the plasma when the frequency is variable. One says that the Langmuir oscillations have a continuous spectrum : for any frequency ω in the range $[0, \max \omega_{pe}(x)]$ one can find a highly localized perturbation of the plasma which oscillates at that frequency. This density pertubation is called a "singular eigenmode".

Due to the fact that $\lambda \ll L$ the energy-carrier in Fig. 1.1 can be described in the geometrical optics (WKB) approximation. Only in the neighborhood of x_T and x_R, where WKB breaks down, one needs to solve a differential equation. The situation in Alfvén wave heating is entirely different, Fig. 1.2. Large scale antennae excite global oscillations of the plasma column. The pertinent wavelength λ in the minor radius direction r is of the order of the inhomogeneity scale length L which is the same as the plasma minor radius r_p. The WKB-method is not applicable. The global modes of the fast magnetosonic wave play the role of the energy-carrier here. The oscillators which store (or dissipate, or convert) the energy are localized shear Alfvén waves in this case. Like the Langmuir waves they have a continuous spectrum as can be seen from their simplest dispersion relation $\omega = v_A(r)k_\parallel(r)$, where $v_A^2(r) = \vec{B}_o^2(r)/4\pi\rho(r)$ is the Alfvén velocity, $\vec{B}_o$ the magnetic field, $\rho(r)$ the mass density, and $k_\parallel(r)$ the wavelength parallel to $\vec{B}_o$.

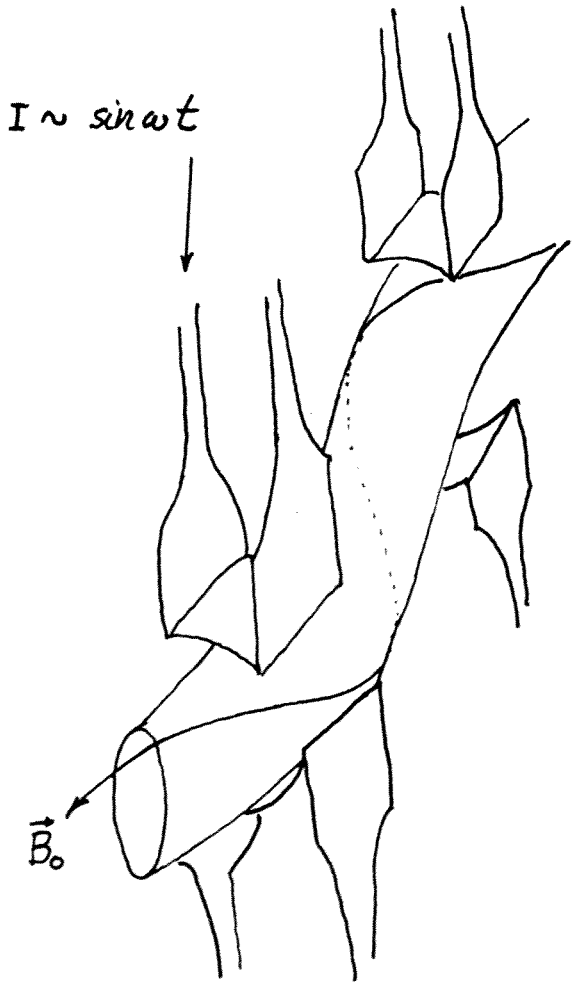

Fig. 1.2

While analytical methods allow one to obtain quite accurate quantitative results in the laser case, not more than qualitative results have been produced analytically in the case of AWH. The main reason is that in AWH all the details of the profiles $B_0(r)$ and $\rho(r)$ enter into the differential equations, whereas in the laser case the profile $n_e(x)$ enters merely into the WKB solution.

The heating in the ion-cyclotron range of frequency resembles strongly AWH since the same energy-carrier, the fast magnetosonic wave, is used. The antennae are of similar size. The frequencies, however, are higher and the radial wavelengths are somewhat shorter. The wavelengths in present-day devices are, however, still comparable with the minor radius r_p; the WKB-approach is highly questionable therefore. Another pronounced difference is that the excitation of global modes is usually avoided. It seems that the resonant absorption process at the ion-ion hybrid layer is strong enough to mask any resonance with a global mode of the column.

The lectures are structured as follows. In chapter 2 we outline the main ideas which are used to model theoretically the laser-plasma interaction. In chapter 3 the cold-plasma equations which can be used for a description of AWH and for ICRF mode-conversion heating are derived in detail. Subsequently, they are presented in different limits which make them appear in different forms known from published literature. At the end of chapter 3 we discuss the different types of singularity possessed by the different equations. Chapter 4 is devoted to the problem of the wave excitation and includes the discussion of the antenna, the vacuum and the boundary conditions. We then solve the eigenvalue problem (free oscillations) in a homogeneous plasma, i.e., we look for the global modes. At the end of chapter 4 their role in heating is discussed on the basis of the results obtained so far. Throughout chapters 2-4 knowledge of neither numerical methods nor the numerically obtained results is required. The numerical methods are briefly discussed in chapter 5. Finally, chapter 6 is a guide through our published work on AWH, and chapter 7 is an outlook to future ICRF-work.

2. LASER-PLASMA INTERACTION

(as the oldest, simplest, and very instructive example of resonant absorption).

2.1 Basic equations

In this chapter we follow largely the description given in Ginzburg's book [3]. A simplified version is given in Ref. 5.

Let us adopt slab geometry. Specifically, we assume a semi-infinite plasma at $x > x_b$ whose density, $n_e(x)$, increases to the right, Fig. 2.1.

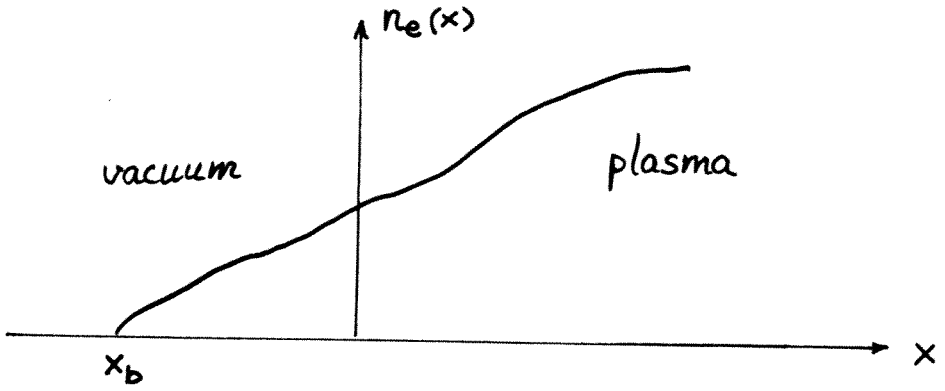

Fig. 2.1

We assume that a plane wave with frequency ω impinges on the plasma. Since the equilibrium depends merely on x, we can represent the wave fields in and outside the plasma by $\sim f(x)\exp[i(k_y y + k_z z - \omega t)]$. The equations for the amplitudes $f(x) = (\vec{E},\vec{B})$ are given by Maxwell's equations in the form

$$\text{rot}\,\vec{B} = -i\frac{\omega}{c}\epsilon\vec{E}, \tag{2.1}$$

$$\text{rot}\,\vec{E} = i\frac{\omega}{c}\vec{B}, \tag{2.2}$$

where the dielectric function ε has the form

$$\epsilon = 1 - \omega_{pe}^2/\omega^2, \tag{2.3}$$

and $\omega_{pe} = \sqrt{4\pi e^2 n_e(x)/m_e}$ is the plasma frequency.

Without loss of generality, we can restrict ourselves to the case where $k_z = 0$. If we use the quantity

$$\vec{H} = i \frac{\omega}{c} \vec{B} \tag{2.4}$$

instead of $\vec{B}$, the eqs (2.1) and (2.2) take the explicit form

$$\left.\begin{aligned} \frac{\omega^2}{c^2} \epsilon E_x &= i k_y H_z \\ \frac{\omega^2}{c^2} \epsilon E_y &= -dH_z/dx \\ \frac{\omega^2}{c^2} \epsilon E_z &= dH_y/dx - i k_y H_x \end{aligned}\right\} \tag{2.5}$$

and

$$\left.\begin{aligned} H_x &= i k_y E_z \\ H_y &= -dE_z/dx \\ H_z &= dE_y/dx - i k_y E_x \end{aligned}\right\}. \tag{2.6}$$

The first equation of (2.5) allows one to eliminate E_x in the last equation of (2.6). Similarly H_x in the last equation of (2.5) may be eliminated using the first equation of (2.6). In doing so one obtains two decoupled systems of equations

$$\left.\begin{aligned} dH_y/dx &= \left(\frac{\omega^2}{c^2}\epsilon - k_y^2\right) E_z \\ dE_z/dx &= -H_y \end{aligned}\right\} \tag{2.7}$$

and

$$\left.\begin{aligned} \frac{\omega^2}{c^2} \epsilon \, dE_y/dx &= \left(\frac{\omega^2}{c^2}\epsilon - k_y^2\right) H_z \\ dH_z/dx &= -\frac{\omega^2}{c^2} \epsilon E_y \end{aligned}\right\}. \tag{2.8}$$

The fact that (2.7) and (2.8) do not have common field components allows us to define two independent polarizations. Traditionally, they

are called s- and p-polarizations :

s-polarization $H_y \neq 0$, $E_z \neq 0$ ($E_y = H_z = 0$) => $E_x = 0$ (2.9),

p-polarization $E_y \neq 0$, $H_z \neq 0$ ($H_y = E_z = 0$) => $H_x = 0$ (2.10).

The waves corresponding to these two polarizations behave quite differently. In the s-polarization, the electric field remains transverse to the direction of wave propagation all along the wave path. This wave is therefore a pure electromagnetic wave.

Formally :

$$\mathrm{div}\,\vec{E} = dE_x/dx + ik_y E_y = 0$$

as can be seen from (2.9). In the p-polarization the components E_x and E_y are different from zero, and therefore, in general, div $\vec{E} \neq 0$. The wave has an electrostatic component and can couple to the Langmuir oscillations. There is another distinct formal difference between the two polarizations : the equations (2.7) are regular whereas the system (2.8) has a singular point at $\varepsilon(x) = 1 - \omega_{pe}^2(x)/\omega^2 = 0$, i.e., at the point where the driving frequency ω equals the local plasma frequency. The case of the p-polarization has much in common with the Alfvén Wave Heating problem. The equations (2.8) have the same structure as the equations pertinent to Alfvén Wave Heating in a plane geometry [6].

2.2 S-polarization

For the sake of completeness, we discuss not only the p-polarization but also the s-polarization. In doing so, it is possible to give an introduction to the analytical theory of wave propagation in weakly inhomogenous media which is one of the theoretical tools in RF heating. Though not very useful for Alfvén Wave heating it is, on the other hand, widely used for ICRF heating to which, after all, Alfvén Wave Heating belongs. This theory is based on the assumption that the pertinent wavelength λ is much smaller than L, the characteristic length of the density variation.

From the eqs (2.7), pertinent to the s-polarization, one can obtain the corresponding 2nd order equation

$$\frac{d^2E_z}{dx^2} + \left(\frac{\omega^2}{c^2}\,\epsilon(x) - k_y^2\right)E_z = 0. \qquad (2.11)$$

In a sufficient distance from the turning point x_T, where $(\omega^2/c^2)\,(x_T) = k_y^2$, this equation can be solved in the approximation of geometrical optics (WKB), i.e.,

$$E_z = \frac{const}{k_x^{1/2}}\,\exp i\left[\int^x k_x dx' + k_y y - \omega t\right], \qquad (2.12)$$

where

$$k_x^2 = \frac{\omega^2}{c^2}\,\epsilon(x) - k_y^2 . \qquad (2.13)$$

The eq. (2.12) holds under the condition $|k'_x| \ll |k_x^2|$ and $|k_x''| \ll |k_x^3|$, that is, away from the turning point x_T and for sufficiently slowly varying $\varepsilon(x)$. In the neighborhood of the turning point one needs an exact solution of eq. (2.11).

Let us assume that the electron density $n_e(x)$ varies linearly in the neighborhood of the turning point. In order to have a unified notation for the s- and the p-polarizations, let us also choose the coordinate system in such a way, that $n_e(x) = (1+x/L)n_o$ with $\omega_{pe}^2(x=0) = \omega_{peo}^2 = 4\pi e^2 n_e(x=0)/m_e = \omega^2$. Using this assumption we can write

$$k_x^2 = \frac{\omega^2}{c^2} - \frac{\omega_{peo}^2}{c^2}\left(1+\frac{x}{L}\right) - k_y^2 = -\frac{\omega_{peo}^2}{c^2}\,\frac{x}{L} - k_y^2 = -k_o^2\frac{x}{L} - k_y^2 . \qquad (2.14)$$

Here $k_o = \omega/c$ denotes the vacuum wavenumber. The turning point is situated at $x_T = -L\,k_y^2/k_o^2 = -L\,\sin^2\theta$ where θ denotes the angle of incidence at the plasma boundary, see Fig. 2.2.

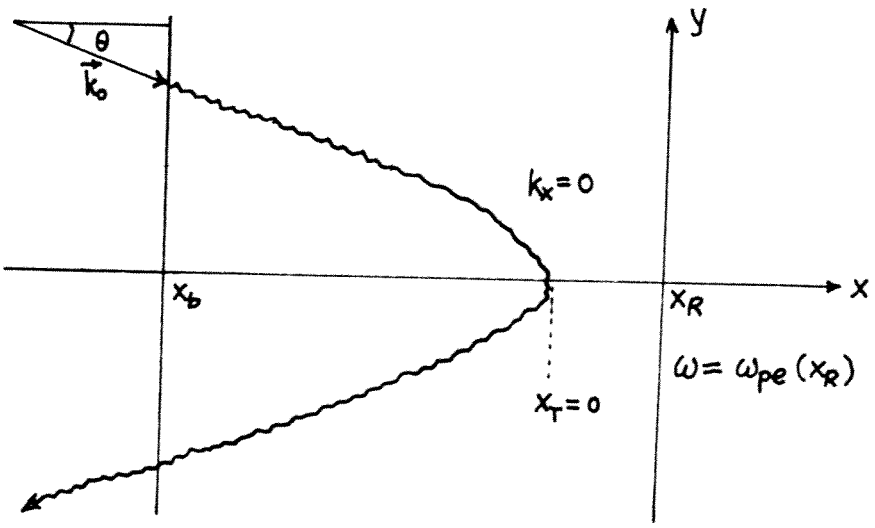

Fig. 2.2 Electromagnetic wave incident on plane slab

The wave equation (2.11) assumes the simplest form under the variable transformation

$$\xi = \left(\frac{k_0^2}{L}\right)^{1/3} (x + L \sin^2\theta) , \tag{2.15}$$

namely,

$$\frac{d^2 E_z}{d\xi^2} - \xi E_z = 0. \tag{2.16}$$

This is the Airy equation.

The two linearly-independent solutions are Ai(ξ) and Bi(ξ) (see Abramowitz and Stegun [7]). Both functions are bounded and oscillatory for $\xi < 0$, and monotonic for $\xi > 0$. Bi(ξ), however, diverges for $\xi \to \infty$ as $\xi^{-1/4}$ exp $(2/3\ \xi^{3/2})$ and must therefore be excluded as a physical solution. The physical solution is given by Ai(ξ), Fig. 2.3, only.

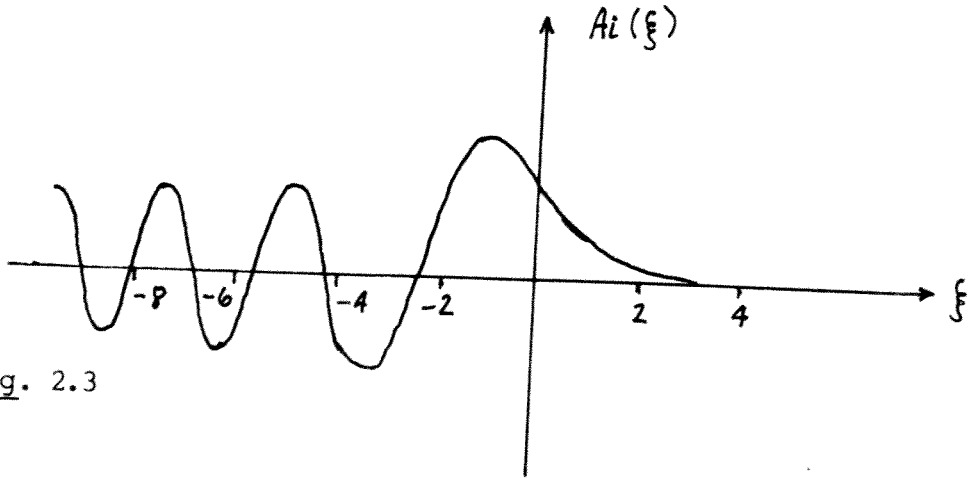

Fig. 2.3

Far away from the turning point, $\xi = 0$, the WKB-approximation is a good approximation. For large-enough ξ we expect therefore that $Ai(\xi)$ has the form of the WKB-solution, eq. (2.12), evaluated with the linear density profile. That this is indeed so, can be seen from the asymptotic expansion of $Ai(\xi)$ and the explicit expression for $\int k_x dx$ using the linear density profile.

For $|\xi| \to \infty$ we have [7]

$$\xi > 0: \quad Ai(\xi) \sim \frac{1}{2}\pi^{-1/2}\xi^{-1/4}\exp\left(-\frac{2}{3}\xi^{3/2}\right), \tag{2.17}$$

$$\xi < 0: \quad Ai(\xi) \sim \pi^{-1/2}\xi^{-1/4}\sin\left[\frac{2}{3}(-\xi)^{3/2} + \frac{\pi}{4}\right]. \tag{2.18}$$

For the identification with the WKB-solution let us first combine (2.14) and (2.15) to

$$k_x^2 = -\left(\frac{k_0^2}{L}\right)^{2/3}\xi. \tag{2.19}$$

We then find by using (2.15) once more

$$\int^x k_x\,dx = \int^\xi \sqrt{-\xi}\,d\xi = -\frac{2}{3}(-\xi)^{3/2}. \tag{2.20}$$

We see that $\xi^{-1/4}$ in (2.17) and (2.18) is the same as $k_x^{-1/2}$ in (2.12) and also that we have the same exponential dependence.

One can now perform the so-called matching procedure where the Airy solution is matched to an in-coming WKB wave of given amplitude, e.g.

$$E_z^{in} = \frac{1}{(-\xi)^{1/4}}\exp\left[-i\frac{2}{3}(-\xi)^{3/2}\right] \tag{2.21}$$

and an out-going wave with an amplitude which is to be determined

$$E_z^{out} = \frac{R}{(-\xi)^{1/4}}\exp\left[i\frac{2}{3}(-\xi)^{3/2}\right]. \tag{2.22}$$

In the present s-polarization case the problem is trivial. We find $R = -i$, or $|R| = 1$, which corresponds to total reflection. This result was to be expected from the fact that in the s-polarization the wave is purely electromagnetic and does not interact with another wave nor does it propagate further into the plasma.

2.3 P-polarization

Let us now try to get an understanding of the coupling between the electromagnetic wave and the Langmuir oscillations. From eqs (2.8) one obtains

$$\frac{d^2H_z}{dx^2} - \frac{\partial\epsilon/\partial x}{\epsilon}\frac{dH_z}{dx} + \left(\frac{\omega^2}{c^2}\epsilon - k_y^2\right)H_z = 0. \qquad (2.23)$$

We remark that if the inhomogeneity is weak, i.e., if $\partial\epsilon/\partial x$ is small in some sense, eq. (2.23) is identical with eq. (2.11) for E_z. For a linear density profile the solutions of eq. (2.23) will be Airy-function-like somewhere between the plasma edge and the turning point.

Eq. (2.23) is more difficult to solve then Airy's equation. We therefore refrain from seeking a solution but discuss it qualitatively (along the lines proposed in Ref. 5). From Airy's equation we know that the characteristic length in the neighborhood of the turning point is $\sim(L/k_o^2)^{1/3}$. Hence the first term in (2.23) has the characteristic size $(k_o^2/L)^{2/3}H_z$, whereas the second term is, using (2.13) and (2.14), $(1/x)dH_z/dx \sim (1/L\sin^2\theta)(k_o^2/L)^{1/3}H_z$. The second term is negligible in the neighborhood of the turning point if $L\sin^2\theta \gg (L/k_o^2)^{1/3}$, i.e., if the distance between the turning point and the resonance point ($\epsilon = 0$, $\omega = \omega_{pe0}$, $x = 0$) is larger than the wavelength near the turning point. In this case the field decays exponentially towards the resonance and the excitation at the resonance point is exponentially small. Conversely, if $(L/k_o^2)^{1/3} \sim L\sin^2\theta$ the field does not decay substantially before reaching the resonance and the resonance has to be taken into account.

The discussion of the resonance is facilitated by the fact that the field component H_z does not diverge at $\epsilon = 0$ as one could guess

from the pertinent 1st order equations (2.8). Noting that under the assumptions made for eq. (2.14) one finds $\varepsilon = -x/L$ and

$$\frac{d^2H_z}{dx^2} - \frac{1}{x}\frac{dH_z}{dx} - \left(\frac{\omega^2}{c^2}\frac{x}{L} + k_y^2\right)H_z = 0. \qquad (2.23')$$

Expanding the solutions around the singular point $x = 0$ [8] one finds one regular, w_1, and one singular solution, w_2,

$$\left.\begin{aligned} w_1 &= x^2 + \frac{1}{8}k_y^2 x^4 + \cdots \\ w_2 &= w_1 \log x + \frac{2}{k_y^2} + \frac{2}{3}\frac{\omega^2}{c^2 L k_y^2}x^3 - \frac{3}{32}k_y^2 x^4 + \cdots \end{aligned}\right\} \qquad (2.24).$$

We conclude that H_z is finite at $x = 0$ with $dH_z/dx = 0$. The value of $H_z(0)$ or rather the ratio of $H_z(0)$ to the incoming wave amplitude at the plasma boundary H_z^{in} can only be obtained from the global solution of (2.23). The result obtained from an approximate solution is given in Ref. 3, more recent results are to be found in Ref. 4. The essence of the results is that $H_z(0)/H_z^{in}$ has a maximum at small angles of incidence, specifically at $(k_o L)^{1/3} \sin\theta \approx 1$ with a height of $\approx (2\pi\, k_o L \sin^2\theta)^{-1/2}$.

We are now prepared to discuss "the excitation of the Langmuir oscillator" near the resonance point. First we deduce from (2.5) and (2.8) the behavior of the electric field components near the singularity :

$$E_x \approx -i\, L \sin\theta\, H_z(0) / k_o x\,, \qquad (2.25)$$

$$E_y \approx L \sin^2\theta\, H_z(0) \log x\,. \qquad (2.26)$$

We see that E_x is the dominant component, it diverges as $1/x$.

This singularity disappears if more physics such as collisions or temperature effects (Langmuir <u>waves</u> instead of mere oscillations) is introduced or, if an initial value problem is solved instead of the driven steady-state problem. Let us first consider collisions. With collisions the dielectric function assumes the form

$$\epsilon = 1 - \frac{\omega_{pe}^2}{\omega(\omega + i\nu)}\,, \qquad (2.27)$$

where ν stands for the electron-ion collision frequency. In the neighborhood of the resonance it becomes $\varepsilon \approx -x/L + i\nu/\omega$ and hence with the help of (2.4) we have instead of (2.25)

$$E_x \approx \sin\theta\, B_z(0) \Big/ \left(\frac{x}{L} - i\,\frac{\nu}{\omega} \right) , \qquad (2.25')$$

which is finite everywhere in $x \in \mathbb{R}$.

Noting from (2.27) that the field suffers from collisional damping with a rate of $\nu/2$ we can calculate the total time-averaged collisional power loss per area

$$P/A = \left\langle -\frac{\partial}{\partial t} 2 \int \frac{E^2}{8\pi}\, dx \right\rangle \approx \frac{\nu}{8\pi} \int |E_x|^2\, dx \qquad (2.28)$$

The explicit factor 2 stems from the fact that the energy density in the Langmuir oscillations is given equally by the electrostatic energy and the particle sloshing energy. On using (2.25') one obtains

$$P/A = L\,\omega_{pe} \sin^2\theta\, \frac{|B_z(0)|^2}{8} \int \frac{\frac{1}{\pi} \left(\frac{\nu}{\omega} L\right)}{x^2 + \left(\frac{\nu}{\omega} L\right)^2}\, dx \, . \qquad (2.28').$$

Here we have the most important result in connection with resonant absorption. Since the integrand is a representation of the δ-function, we see that the absorbed power does not depend on the strength of the collisions (at least as long as they are not too frequent to invalidate our local investigation around the resonant point). All they determine is the height and the width of the resonant layer. If this layer became too broad the local approximation would break down. In mathematically formal papers on resonant absorption collisions are even not mentioned. It is sufficient to use the argument of causality which prescribes the manner in which poles have to be treated.

In an initial-value approach, where causality is automatically satisfied a problem never arises. Had we tackled the present problem via a solution of the pertinent equations of motion in time we would have found that the field amplitude at the resonance grows linearly in time whereas the width of the resonance decreases as $1/t$.

The energy content in the resonance layer therefore would grow linearly in time. This process of energy accumulation proceeds until the collisional damping balances the energy flow into the resonant region. The quantitative value of the energy flow into the region does not depend on the presence of the collisions at all. Without collisions one could name the phenomenon "resonant accumulation" of energy instead of resonant absorption [9,10].

To complete this introductory chapter on resonant absorption let us consider the effect of finite temperature following Ref. 5. The primary effect of temperature is to introduce spatial dispersion into the dielectric function

$$\epsilon = 1 - \frac{\omega_{pe}^2}{\omega^2}\left(1 + 3k^2\lambda_d^2\right) . \tag{2.29}$$

This result is obtained for a plane wave ~exp(ikx) in a homogeneous medium. In the general case of an inhomogeneous medium k has to be replaced by d/dx with the result that the first equation of (2.5) is now a differential equation and not simply an algebraic equation like (2.25). Using (2.4) and the fact that $x/L \ll 1$ and $k^2\lambda_d^2 \ll 1$ we obtain approximately

$$3\lambda_d^2 \frac{d^2E_x}{dx^2} - \frac{x}{L}E_x = -B_z(0)\sin\theta . \tag{2.30}$$

For vanishing temperature, i.e., $\lambda_d \to 0$ eq. (2.30) reduces to (2.25) as expected. Eq. (2.30) has the form of an inhomogeneous Airy equation. This time it describes Langmuir waves generated in the resonant region and propagating to the left towards the plasma boundary. Near the resonance their characteristic wavelength Δx is $(L\ \lambda_d^2)^{1/3}$. The field reaches a maximum height of approximately $\lambda_d^2\ E_{max}/\Delta x^2 \approx B_z(0)\ \sin\theta$ or

$$E_{max} \approx B_z(0)\sin\theta\ \left(L/\lambda_d\right)^{2/3}, \tag{2.31}$$

respectively. The energy flux, S, away from the resonance layer can be estimated from $S = v_g\ (1/8\pi)\ |E_x|^2$, where $v_g = 3k\ \lambda_d^2\omega_{pe}$ denotes the group velocity. Ignoring the numerical factors we obtain

$$S \approx L\,\omega_{pe}\,\sin^2\theta\,\frac{|B_z(0)|^2}{8\pi}\,, \qquad (2.32)$$

a quantity which has the same order of magnitude as the power dissipated by collisions, eq. (2.28'). In a real plasma it will be a question of parameters which phenomenon, dissipation and subsequent heat transport or dispersion, takes care of the evacuation of the energy flowing into the resonant layer.

2.4 Remarks on papers directly relevant to Alfvén Wave Heating

The most important sources of the original works on Alfvén Wave Heating by Grossmann and Tataronis [11] were the papers by Barston [12] and Sedlaček [13]. Barston discussed with a considerable amount of mathematical rigor the second order differential equation for E_y which follows from (2.8) :

$$\frac{d}{dx}\,\frac{\omega^2\epsilon/c^2}{\omega^2\epsilon/c^2 - k_y^2}\,\frac{dE_y}{dx} + \frac{\omega^2}{c^2}\,\epsilon\,E_y = 0. \qquad (2.33)$$

Barston neglected the contribution due to the incoming electromagnetic wave by approximating the denominator by $-k_y^2$ and solved the problem as a normal-mode or eigenvalue problem which yields a continuous spectrum and singular eigenfunctions. Sedlaček then tackled the problem as an initial value problem and showed the equivalence of the two approaches. The complexity of the mathematics especially in Sedlaček's paper demonstrates the absolute need for numerical solutions in the case where WKB is not applicable. Numerical solutions can be easily obtained and provide, after all, at least as much physical insight as complicated analytical treatments.

Hasegawa and Chen's [6] initial equation [their eq. (15) in the PRL-paper] reduces in the limit of low β to an equation which has exactly the form of (2.33). They were able to cope analytically with both the energy carrier wave and the absorbing wave (or rather oscillation) in the case of a linear profile of ε in slab geometry.

3. COLD-PLASMA EQUATIONS RELEVANT TO ALFVEN AND ICRF HEATING

3.1 Derivation of the basic equations [17]

3.1.1 Preliminary remarks

Historically, Alfvén Wave Heating has first been treated in the approximation of ideal MHD [6,11]. It has been found, however, that several features of existing experiments [14,15,16] could not been explained by ideal MHD theory. Subsequently it was possible to model these features within the framework of cold-plasma theory, or equivalently within the framework of MHD including the Hall term in Ohm's law [17, 2]. The new effect included in this model was that due to a finite value of ω/ω_{ci}. Since finite-β effects are unimportant in a theory of Alfvén Wave Heating for tokamaks we derive here directly the relevant cold-plasma equations. In the next section (sect. 3.2) we shall discuss the low-β MHD limit in order to provide a complete picture. The cold-plasma equations have the additional advantage over those of ideal MHD in that they are pertinent to ICRF-heating of a multi-species plasma in the mode-conversion scenario.

Also, we confine ourselves to cylindrical geometry. The equations relevant to slab geometry will be obtained by simple arguments in the next section (sect. 3.2). As to toroidal geometry, it has many features in common with cylindrical geometry. Some specifically toroidal effects will be touched upon in the last chapter (chapter 6).

3.1.2 Equilibrium and approximations

Before deriving the linear wave equations we have to specifiy the state of the plasma we intend to perturb, i.e., the equilibrium. Let us start by defining the equilibrium quantities as functions of the radial cylinder coordinate r. We will denote by $\vec{B}_o(r)$ the magnetic field, and by $n_{io}(r)$, $n_{eo}(r)$, $\vec{v}_{io}(r)$, $\vec{v}_{eo}(r)$ the ion and electron densities and mean velocities, respectively. The index i runs over all ion species with charges q_i and masses m_i. We assume the electric field

$\vec{E}_0$ to be zero. These quantities have to satisfy the stationary equations of motion

$$m_e n_{e0} (\vec{v}_{e0} \cdot \nabla) \vec{v}_{e0} = - \nabla p_{e0} - n_{e0} \frac{e}{c} \vec{v}_{e0} \times \vec{B}_0 , \qquad (3.1)$$

$$m_i n_{i0} (\vec{v}_{i0} \cdot \nabla) \vec{v}_{i0} = - \nabla p_{i0} + n_{i0} \frac{q_i}{c} \vec{v}_{i0} \times \vec{B}_0 , \qquad (3.2)$$

and the quasineutrality condition

$$\sum_i q_i n_{i0} = n_{e0} . \qquad (3.3)$$

The left-hand sides reduce to $-\vec{e}_r mnv_{0\theta}^2/r$ since div $n_0\vec{v}_0 = 0$ implies $(\vec{v}_{e0}\cdot\vec{e}_r) = (\vec{v}_{i0}\cdot\vec{e}_r) = 0$.

Now we introduce the essential approximations for the derivation of our equations. We intend to neglect systematically terms of order β, i.e. we neglect the pressure terms $\nabla p_{e0} \approx \nabla p_{i0} \approx 0$. If we make the additional approximation $B_{0\theta}/B_{0z} \ll 1$, $B_{0z} \approx$ const (tokamak approximation), terms containing $v_{0\theta}^2$ are also negligible. With this the eqs (3.1) and (3.2) reduce to $\vec{v}_{e0} \times \vec{B}_0 = 0$ and $\vec{v}_{i0} \times \vec{B}_0 = 0$, i.e. the velocities are parallel to the field (force free !!). Finally we suppress the equilibrium mass flow by setting $\vec{v}_{i0} = 0$.

The appoximations which we will need in the remainder are

$$B_{0z} \approx \text{const}, \quad \left|\frac{B_{0\theta}}{B_0}\right| \ll 1, \quad \vec{v}_{e0} = V_0 \vec{e}_{\parallel}, \quad |V_0| \sim \left|\frac{B_{0\theta}}{B_0}\right|, \quad \vec{e}_{\parallel} = \frac{\vec{B}_0}{B_0} , \qquad (3.4)$$

and we will work up to 1st order in $B_{0\theta}/B_0$ or V_0 respectively. That this is important, we know from our original numerical MHD studies. The terms containing V_0 we will call the "equilibrium-current terms".

3.1.3 Perturbed current

If we were willing to drop terms of the order $B_{0\theta}/B_0$ all together the expression for the perturbed current could be copied from a text book. Since we are not, we have to derive it.

Let us start with the electrons and calculate their perturbed velocity v_e in terms of the perturbed fields $\vec{E}$ and $\vec{B}$. First we assume that their mass is negligible and obtain from the equation of motion

$$0 = \vec{E} + \frac{1}{c}\vec{v}_e \times \vec{B}_0 + \frac{V_0}{c}\vec{e}_{\parallel} \times \vec{B} \,. \tag{3.5}$$

We have no equation for $\vec{e}_{\parallel}\cdot\vec{v}_e$ because we have assumed $m_e = 0$, i.e., infinite mobility along the magnetic field. Consequently $\vec{e}_{\parallel}\cdot\vec{E} = 0$. All this is reasonable as long as the driving frequency ω is not too high; specifically $\omega \ll \omega_{LH}$ (lower hybrid). Note that we will never need $\vec{e}_{\parallel}\cdot\vec{v}_e = v_{e\parallel}$. The operation $e_{\parallel}x$ on eq. (3.5) yields

$$\vec{v}_e - v_{e\parallel}\vec{e}_{\parallel} = -c\,\frac{\vec{e}_{\parallel}\times\vec{E}}{B_0} + \frac{V_0}{B_0}\left(\vec{B} - B_{\parallel}\vec{e}_{\parallel}\right). \tag{3.6}$$

The first term on the right-hand side is the ExB-drift, the second term is the equilibrium current term.

In Maxwell's equations we will need the current in perpendicular direction in the form $(4\pi/\omega)\vec{j}$. We therefore directly calculate the electron current

$$\vec{j}_e - j_{e\parallel}\vec{e}_{\parallel} = -e n_{e0}\left(\vec{v}_e - v_{e\parallel}\vec{e}_{\parallel}\right) \tag{3.7}$$

in this form. From eq. (3.6) one finds

$$\frac{4\pi}{\omega}\left(\vec{j}_e - j_{e\parallel}\vec{e}_{\parallel}\right) = \frac{4\pi e n_{e0} c}{\omega B_0}\vec{e}_{\parallel}\times\vec{E} + \frac{4\pi}{\omega}\left(-e n_{e0} V_0\right)\frac{\vec{B} - B_{\parallel}\vec{e}_{\parallel}}{B_0} \,. \tag{3.8}$$

To give (3.8) its final form we remark that $4\pi e n_{0e} c/B_0 = \omega_{pi}^2/\omega_{ci}$, where ω_{pi} and ω_{ci} are the ion-plasma and the ion-cyclotron frequencies, respectively, and $-e n_{e0} V_0 = j_{0\parallel} = c/4\pi\ \mathrm{rot}_{\parallel}\vec{B}_0$ is the equilibrium current. Hence,

$$\frac{4\pi}{\omega}\left(\vec{j}_e - j_{e\parallel}\vec{e}_{\parallel}\right) = \sum_i \frac{\omega_{pi}^2}{\omega\,\omega_{ci}}\vec{e}_{\parallel}\times\vec{E} + \frac{c}{\omega}\,\frac{\mathrm{rot}_{\parallel}B_0}{B_0}\left(\vec{B} - B_{\parallel}\vec{e}_{\parallel}\right). \tag{3.9}$$

Now let us turn to the ions. Since they do not carry any equilibrium current, their perturbed velocities and current are given by the text-book expressions. For completeness we give at least a few intermediate expressions. The equation of motion is

$$-i\omega \vec{v}_i = \frac{q_i}{m_i} \vec{E} + \frac{q_i}{m_i c} \vec{v}_i \times \vec{B}_0 , \qquad (3.10)$$

where we have assumed that the perturbed quantities vary as $\exp[i(m\theta+kz-\omega t)]$. First we note that $\vec{e}_\parallel \cdot \vec{v}_i = 0$ because $\vec{e}_\parallel \cdot \vec{E} = 0$. The operation $\vec{B}_0 \times$ on eq. (3.10) and the replacement of the resulting $\vec{B}_0 \times \vec{v}_i$ term on the left-hand side by eq. (3.10) yields

$$\vec{v}_i = -i \frac{\frac{\omega}{\omega_{ci}}}{1-\left(\frac{\omega}{\omega_{ci}}\right)^2} c \frac{\vec{E}}{B_0} - \frac{1}{1-\left(\frac{\omega}{\omega_{ci}}\right)^2} c \frac{\vec{e}_\parallel \times \vec{E}}{B_0} \qquad (3.11)$$

The ion current $\vec{j}_i = q_i n_{io} \vec{v}_i$ is then

$$\frac{4\pi}{\omega} \vec{j}_i = -i \frac{\left(\frac{\omega_{pi}}{\omega_{ci}}\right)^2}{1-\left(\frac{\omega}{\omega_{ci}}\right)^2} \vec{E} - \frac{\frac{\omega_{pi}^2}{\omega\,\omega_{ci}}}{1-\left(\frac{\omega}{\omega_{ci}}\right)^2} \vec{e}_\parallel \times \vec{E} . \qquad (3.12)$$

For the electric induction

$$\vec{\epsilon} \cdot \vec{E} = \vec{E} + i \frac{4\pi}{\omega} \left(\vec{j}_e - j_{e\parallel} \vec{e}_\parallel + \sum_i \vec{j}_i \right) \qquad (3.13)$$

we obtain

$$\vec{\epsilon} \cdot \vec{E} = S \vec{E} + i D \vec{e}_\parallel \times \vec{E} + i \frac{c}{\omega} \frac{\mathrm{rot}_\parallel B_0}{B_0} \left(\vec{B} - B_\parallel \vec{e}_\parallel \right) . \qquad (3.14)$$

The quantities S and D are defined as in Stix's book [18] (under the assumption $m_e = 0$) :

$$S = 1 + \sum_i \frac{\left(\frac{\omega_{pi}}{\omega_{ci}}\right)^2}{1-\left(\frac{\omega}{\omega_{ci}}\right)^2} = 1 + \frac{c^2}{v_A^2} \sum_i \frac{f_i}{1-\left(\frac{\omega}{\omega_{ci}}\right)^2} , \qquad (3.15)$$

$$D = -\sum_i \frac{\left(\frac{\omega_{pi}}{\omega_{ci}}\right)^2 \frac{\omega}{\omega_{ci}}}{1-\left(\frac{\omega}{\omega_{ci}}\right)^2} = -\frac{c^2}{v_A^2} \sum_i \frac{f_i \frac{\omega}{\omega_{ci}}}{1-\left(\frac{\omega}{\omega_{ci}}\right)^2} . \qquad (3.16)$$

The expressions containing the mass fraction $f_i = n_{io}m_i / \sum n_{io}m_i$ follow from the relation $\omega_{pi}^2/\omega_{ci}^2 = (c^2/v_A^2)f_i$, where v_A denotes the Alfvén velocity, $v_A^2 = B_o^2/(4\pi \sum n_{io}m_i)$. Note that in general both f_i and v_A are functions of radial position. The cyclotron frequency, on the other hand, does not depend on r in the low-β, cylindrical, tokamak approximation. In slab geometry, ω_{ci} may depend on the coordinate x.

Let us remark that the equilibrium-current term in eq. (3.14) is a simple additive correction to the classical dielectric tensor. This feature remains true in toroidal geometry.

3.1.4 Magnetic coordinates

Usually the discussion of physics is simple if one is able to describe the phenomena in question with simple equations. Here, our goal should be therefore to derive wave equations with the simplest possible structure.

As a guideline we can take ideal MHD in cylindrical geometry where it was possible to bring the equations into a very transparent form [19] by using the appropriate variables : $\xi_r = (i/\omega)v_r$, the displacement in radial direction, and $p = \vec{B}_o \cdot \vec{B}$, the perturbed pressure. We would therefore expect $B_\parallel$ and E (from MHD Ohm's law : $E = v_r B_o/c$) to be good variables. The direction $\vec{e}_\perp$ is defined by $\vec{e}_\perp = \vec{e}_\parallel \times \vec{e}_r$.

We shall write the Maxwell equations in the orthogonal right-handed curvilinear coordinate system defined by

$$\vec{e}_r, \quad \vec{e}_\perp = \vec{e}_\parallel \times \vec{e}_r, \quad \vec{e}_\parallel = \vec{B}_o / B_o . \tag{3.17}$$

Any vector in this system has the representation

$$\vec{A} = A_r \vec{e}_r + A_\perp \vec{e}_\perp + A_\parallel \vec{e}_\parallel = \sum_\mu A_\mu \vec{e}_\mu . \tag{3.18}$$

For Maxwell's equations we will need

$$\mathrm{rot}\,\vec{A} = \sum_{\mu} \left(A_\mu \,\mathrm{rot}\,\vec{e}_\mu - \vec{e}_\mu \times \nabla A_\mu \right). \tag{3.19}$$

Since the equilibrium is specified in the usual cylindrical coordinates, $(\vec{e}_r,\vec{e}_\theta,\vec{e}_z)$, we need the transformation formulae between the latter and the magnetic coordinates, eq. (3.17). Projection of e_θ and e_z onto the system (3.17) yields to first order in $|B_{0\theta}/B_0|$

$$\left.\begin{aligned} \vec{e}_\theta &= \vec{e}_\perp + \frac{B_{0\theta}}{B_0}\,\vec{e}_\parallel , \\ \vec{e}_z &= -\frac{B_{0\theta}}{B_0}\,\vec{e}_\perp + \vec{e}_\parallel . \end{aligned}\right\} \tag{3.20}$$

Likewise, projection of $\vec{e}_\perp$ and $\vec{e}_\parallel$ onto the cylindrical system produces

$$\left.\begin{aligned} \vec{e}_\perp &= \vec{e}_\theta - \frac{B_{0\theta}}{B_0}\,\vec{e}_z , \\ \vec{e}_\parallel &= \frac{B_{0\theta}}{B_0}\,\vec{e}_\theta + \vec{e}_z . \end{aligned}\right\} \tag{3.21}$$

Next we need the rots of the basis vectors, eq. (3.17). A simple way is to go via

$$\mathrm{rot}\,\vec{e}_r = 0, \quad \mathrm{rot}\,\vec{e}_\theta = \frac{\vec{e}_z}{r}, \quad \mathrm{rot}\,\vec{e}_z = 0. \tag{3.22}$$

To 1st order in $|B_{0\theta}/B_0|$ we find from (3.21) and (3.22) using (3.19) ($\mu = \theta,z$)

$$\left.\begin{aligned} \mathrm{rot}\,\vec{e}_\perp &= \mathrm{rot}\,\vec{e}_\theta + \vec{e}_z \times \nabla \frac{B_{0\theta}}{B_0} = r\left(\frac{1}{r}\frac{B_{0\theta}}{B_0}\right)'\vec{e}_\perp + \frac{1}{r}\,\vec{e}_\parallel , \\ \mathrm{rot}\,\vec{e}_\parallel &= \frac{B_{0\theta}}{B_0}\,\mathrm{rot}\,\vec{e}_\theta - \vec{e}_\theta \times \nabla \frac{B_{0\theta}}{B_0} = \frac{1}{r}\left(r\,\frac{B_{0\theta}}{B_0}\right)'\vec{e}_\parallel . \end{aligned}\right\} \tag{3.23}$$

Here the prime denotes d/dr.

The gradient ∇ acting on the perturbed quantities is (d/dr,i m/r, ik) in cylindrical coordinates and ($d/dr, ik_\perp, ik_\parallel$) in magnetic coordinates if we define

$$k_\perp = \frac{m}{r} - k\,\frac{B_{0\theta}}{B_0}, \qquad k_\parallel = \frac{m}{r}\,\frac{B_{0\theta}}{B_0} + k \tag{3.24}$$

We can now obtain $\mathrm{rot}\vec{A}$ in magnetic coordinates by using eqs (3.19), (3.20), (3.23) and (3.24). In components we have

$$\left.\begin{aligned} \mathrm{rot}_r \vec{A} &= i k_\perp A_\parallel - i k_\parallel A_\perp , \\ \mathrm{rot}_\perp \vec{A} &= i k_\parallel A_r - A_\parallel' + r\left(\frac{1}{r}\frac{B_{0\theta}}{B_0}\right)' A_\perp , \\ \mathrm{rot}_\parallel \vec{A} &= \frac{1}{r}(rA_\perp)' - i k_\perp A_r + \frac{1}{r}\left(r\frac{B_{0\theta}}{B_0}\right)' A_\parallel . \end{aligned}\right\} \tag{3.25}$$

correct up to 1st order in $|B_{0\theta}/B_0|$.

3.1.5 Maxwell's equations

Maxwell's equations can be written as

$$\mathrm{rot}\,\vec{B} = -i\,\frac{\omega}{c}\,\vec{\vec{\epsilon}}\cdot\vec{E}, \tag{3.26}$$

$$\mathrm{rot}\,\vec{E} = i\,\frac{\omega}{c}\,\vec{B}, \tag{3.27}$$

or equivalently

$$\mathrm{rotrot}\,\vec{E} = \frac{\omega^2}{c^2}\,\vec{\vec{\epsilon}}\cdot\vec{E} . \tag{3.28}$$

Eqs (3.14), (3.27) and (3.28) provide all the bits we need for the construction of the wave equation. For consistency and for simplicity reasons we use Maxwell's equations in the form eq. (3.28) although we ultimately aim at the variables $E_\perp$ and $B_\parallel$. Using twice the relations (3.25) we can write the components of $\mathrm{rotrot}\vec{E}$:

$$\left.\begin{aligned} \mathrm{rot}_r \mathrm{rot}\,\vec{E} &= (k_\perp^2 + k_\parallel^2) E_r + \frac{ik_\perp}{r}(rE_\perp)' - ik_\parallel r\left(\frac{1}{r}\frac{B_{0\theta}}{B_0}\right)' E_\perp , \\ \mathrm{rot}_\perp \mathrm{rot}\,\vec{E} &= k_\parallel^2 E_\perp - \frac{d}{dr}\left[-ik_\perp E_r + \frac{1}{r}(rE_\perp)'\right] + ik_\parallel r\left(\frac{1}{r}\frac{B_{0\theta}}{B_0}\right)' E_r . \end{aligned}\right\} \qquad (3.29)$$

The two components of the electric induction can be obtained from eq. (3.14) by means of eqs (3.27) and (3.25)

$$\left.\begin{aligned} \left(\frac{\omega^2}{c^2}\vec{\epsilon}\cdot\vec{E}\right)_r &= \frac{\omega^2}{c^2} S E_r - i\frac{\omega^2}{c^2} D E_\perp + \frac{1}{r}\left(r\frac{B_{0\theta}}{B_0}\right)'(-ik_\parallel E_\perp), \\ \left(\frac{\omega^2}{c^2}\vec{\epsilon}\cdot\vec{E}\right)_\perp &= \frac{\omega^2}{c^2} S E_\perp + i\frac{\omega^2}{c^2} D E_r + \frac{1}{r}\left(r\frac{B_{0\theta}}{B_0}\right)' ik_\parallel E_r . \end{aligned}\right\} \qquad (3.30)$$

Noting that

$$\frac{1}{r}\left(r\frac{B_{0\theta}}{B_0}\right)' - r\left(\frac{1}{r}\frac{B_{0\theta}}{B_0}\right)' = 2\frac{B_{0\theta}}{r B_0}$$

we obtain from (3.28) - (3.30) :

$$\left.\begin{aligned} ik_\perp \frac{1}{r}(rE_\perp)' &= (A - k_\perp^2) E_r + iG E_\perp , \\ \frac{d}{dr}\left[\frac{1}{r}(rE_\perp)' - ik_\perp E_r\right] &= iG E_r - A E_\perp , \end{aligned}\right\} \qquad (3.31)$$

where

$$\left.\begin{aligned} A &= \frac{\omega^2}{c^2} S - k_\parallel^2 = \frac{\omega^2}{c^2} + \frac{\omega^2}{v_A^2}\sum_i \frac{f_i}{1 - \frac{\omega^2}{\omega_{ci}^2}} - k_\parallel^2 , \\ G &= -\frac{\omega^2}{c^2} D - \frac{2k_\parallel}{r}\frac{B_{0\theta}}{B_0} = \frac{\omega^2}{v_A^2}\sum_i \frac{f_i \frac{\omega}{\omega_{ci}}}{1 - \frac{\omega^2}{\omega_{ci}^2}} - \frac{2k_\parallel}{r}\frac{B_{0\theta}}{B_0} . \end{aligned}\right\} \qquad (3.32)$$

Note that A=0 represents the dispersion relation of the Alfvén wave. The term ω^2/c^2 is often neglected arguing that $c \gg v_A$. Note also that G = 0 if $\omega/\omega_{ci} = 0$ and the equilibrium current term is neglected ! We shall discuss this approximation later on.

The wave equations (3.31) assume a much more transparent form if $B_\parallel$ instead of E_r is used, as we have anticipated. From (3.27) and (3.25) we have

$$\frac{i\omega}{c} B_{\parallel} = \frac{1}{r}(rE_{\perp})' - ik_{\perp} E_r \,. \tag{3.33}$$

When this is used to eliminate E_r we find from (3.31)

$$A \frac{1}{r}(rE_{\perp})' = k_{\perp} G E_{\perp} + (A - k_{\perp}^2) i \frac{\omega}{c} B_{\parallel} \tag{3.34}$$

$$A \left(\frac{i\omega}{c} B_{\parallel}\right)' = (G^2 - A^2) E_{\perp} - k_{\perp} G \, i \frac{\omega}{c} B_{\parallel} \tag{3.35}$$

The eqs (3.34) and (3.35) are the basic equations which we shall use for the discussion of AWH.

3.1.6 Preliminary discussion of the wave equations

The wave equations, (3.34) and (3.35), are singular at r=0 and may be singular at the points $r=r_0$, where $A(r_0)=0$.

One more remark is in order. It concerns the appearance of G^2 in eq. (3.35). The expression G^2, eq. (3.32), contains a term of the order $(B_{0\theta}/B_0)^2$ which we have considered to be negligible all along our derivation of the equations. This term may <u>not</u> be neglected here. There are good reasons for this somewhat astonishing claim. The first reason is mathematical. The term in question affects the nature of the singularities at r=0 and at $r=r_0$. Let us show this fact explicitly for the singularity at the origin by deriving the pertinent indicial equation from eqs (3.34) and 3.35). If we exclude the pathological cases A(o) = 0 and G(o) = 0, for $r \to 0$ we have $k_{\perp} \sim m/r$, $k_{\parallel}$ finite, $A \sim a$ and $G \sim g$, both finite. By using $rE_{\perp} = e_0 r^{\alpha}$ and $(i\omega/c)B_{\parallel} = h_0 r^{\alpha}$ we obtain from eqs (3.34) and (3.35)

$$\begin{aligned} (mg - \alpha a) f_0 - m^2 h_0 &= 0 \\ (g^2 - a^2) f_0 - (mg + \alpha a) h_0 &= 0 \end{aligned} \tag{3.36}$$

The homogeneous system (3.36) has a nontrivial solution for f_0 and h_0 if the determinant vanishes, that is, if $a^2(\alpha^2 - m^2) = 0$. The indicial equation, $\alpha^2 = m^2$, indicates that there is one regular and one singular

solution. The regular solution behaves like $\sim r^m$ near the origin. The same conclusion can be drawn from an analysis of eq. (3.31). Had we, however, neglected the term proportional to $B_{o\theta}/B_o{}^2$ in G^2 we would have concluded from eqs (3.34) and (3.35) that α is, in a best case, a fractional number. Similarly, the singularity at $r=r_0$, where the indicial equation is $\alpha^2=0$, would change, leading again to a fractional number. This singularity would even not describe resonant absorption.

We are now convinced that the term $\sim|B_{o\theta}/B_o|^2$ in G^2 is important in eqs (3.34) and (3.35). We, however, still feel uneasy due to the fact that we have neglected plenty of terms of order $|B_{o\theta}/B_o|^2$ in the course of the derivation of eqs (3.34) and (3.35). Could they have any importance ? It seems not. We have performed numerical experiments using finite-β ideal MHD equations [19]. These equations contain many terms proportional to $|B_{o\theta}/B_o|^2$. We have found that only the term corresponding to that in G^2 had an influence on results relevant to AWH of low-β tokamaks. The profound reason seems to be that this term has a special origin (curvature of magnetic field lines [21]) whereas the others are pressure or geometric terms. In this connection it is interesting to note that this term does not appear in slab geometry with shear [1,6,24].

3.2 The wave equations in different limits

3.2.1 Second order equation

For the discussion of the singularities (sect. 3.3) it is conventional to use the second order differential equation [8] instead of the system of first order equations. The second order equation corresponding to eqs (3.34) and (3.35) is readily obtained by acting with $(d/dr)\,[1/(A-k_\perp{}^2)]$ on eq. (3.34) and eliminating $B_\parallel$

$$\frac{d}{dr}\frac{A}{A-k_\perp^2}\frac{1}{r}\frac{d}{dr}(rE_\perp)+\left[\frac{A}{r}-\frac{G^2}{A-k_\perp^2}\frac{1}{r}-\left\{\frac{d}{dr}\left(\frac{k_\perp G}{A-k_\perp^2}\frac{1}{r}\right)\right\}\right]rE_\perp=0. \quad (3.37)$$

The points where $A - k_\perp^2 = 0$ are only apparently singular as may be seen from eqs (3.34) and (3.35) [19,20].

3.2.2 MHD-limit

MHD implies $\omega/\omega_{ci} = 0$ and $c \gg v_A$. The quantities A and G reduce to the classical dispersion relation of the Alfvén wave, $A = \omega^2/v_A^2 - k_\parallel^2$, and to the equilibrium-current term, $G = -2k_\parallel B_{0\theta}/(rB_0)$. The resulting wave equations have been discussed in Ref. 21.

3.2.3 Slab geometry

Tracing back to eq. (3.25) the origin of the equilibrium-current term in G, we remark that it is due to cylindrical geometry. Hence in plane slab geometry, G reduces to the homogeneous plasma expression

$$G = \frac{\omega^2}{v_A^2} \sum_i \frac{f_i \frac{\omega}{\omega_{ci}}}{1 - \frac{\omega^2}{\omega_{ci}^2}} \quad , \tag{3.38}$$

with space-dependent $v_A(x)$ and $f_i(x)$. In plane geometry (x,y,z) the operators d/dr, $r(d/dr)r^{-1}$, $r^{-1}(d/dr)r$ in eqs (3.34), (3.35) and (3.37) are replaced by d/dx. The wave vectors m/r and k become k_y and k_z.

After these transformations we can compare our results with results in the literature. Equations (3.34) and (3.35) have exactly the form of eqs (4) and (5) in Ref. 20. Equation (3.37) differs, however, from eq. (31) in Stix and Swanson's handbook article [22]. The reason for which they obtained second-order derivatives of the equilibrium quantities is unclear. It must have to do with the limit $m_e \to 0$ which they take only at the end of their calculations. From their equation they conclude that $A - k_\perp^2 = 0$ is a weak singularity which contradicts even ideal MHD.

If additionally we take the MHD-limit we find from (3.37) Hasegawa and Chen's equation [6] in its low-β limit.

$$\frac{d}{dx} \frac{A}{A - k_\perp^2} \frac{dE_\perp}{dx} + A E_\perp = 0. \tag{3.39}$$

This equation has the same form as eq. (2.33) and can be discussed along the same lines.

It is interesting to note that in slab geometry and on the basis of our equations one cannot find the MHD instabilities. Knowing that these instabilities can be modelled in slab geometry by introducting a gravity term into the equation of motion, eq. (3.10), and also knowing that the stable kink mode has something to do with AWH [23], we have extensively investigated such a model [24]. The results were somewhere between success and failure. Certain features of AWH could be modelled and others not.

3.2.4 Belt geometry

For ICRF-heating of tokamaks it is essential to model the 1/R dependence of the toroidal magnetic field, where R denotes the distance from the symmetry axis. For this reason slab geometry with $B_{oz}(x)$ is usually adopted, as long as one wants to avoid full toroidal geometry. There is, however, an intermediate model which takes at least one toroidal feature into account, the "belt geometry" [25]. In this model $B_{o\theta}(r)$, or rather $B_{o\theta}(R)$, plays the role of the toroidal field. Under the assumption $B_{oz} = 0$ and $k = 0$ equations similar to eqs (3.34) and (3.35) are obtained [25].

3.2.5 Homogeneous current-carrying plasma cylinder

Let us assume that all the densities n_{io} are constant and that the plasma is carrying a constant current density j_{oz}. We then have $B_{o\theta}/r = 2\pi/c\ j_{oz}$. From the definitions of $k_\parallel$, A and G, eqs (3.24) and (3.32), we find that these quantities are constant as well. We can now "almost" derive a Bessel-equation for $B_\parallel$ by multiplying eq. (3.35) by $(d/dr)r/(G^2-A^2)$ and eliminating $E_\perp$:

$$\frac{1}{r}\frac{d}{dr}\, r\, \frac{dB_\parallel}{dr} + \left[A - k_\perp^2 - \frac{G^2}{A} + \frac{G}{A}\frac{1}{r}\frac{d}{dr}(rk_\perp)\right] B_\parallel = 0. \qquad (3.40)$$

Since $k_\perp^2 = m^2/r^2 - 2k(m/r)(B_{o\theta}/B_o)$ to first order in $B_{o\theta}/B_o$ we have a Bessel-equation. It would be interesting to rederive eq. (3.40) making the assumption of homogeneity from the start and working up to 2nd order in $B_{o\theta}/B_o$. We surmise that the result would also be a Bessel equation as in the MHD limit [26].

3.3 Type of singular solutions

Here we determine the behaviour of the wave fields in the neighborhood of the singular points r_o, defined by $A(r_o) = 0$. We will carry out this investigation on the basis of eq. (3.37). Once we know the behaviour of $E_\perp$, that of the other field components is easy to obtain. Let us write eq. (3.37) in the form

$$\frac{d}{dx}\mathfrak{D}\frac{d}{dx}(rE_\perp) + Vr E_\perp = 0 , \qquad (3.41)$$

where $x = r - r_o$ and the definition of $\mathfrak{D}$ and V can be obtained by identification with eq. (3.37).

For our discussion it is sufficient to expand $\mathfrak{D}$ and V to the first two terms in x : $\mathfrak{D} \approx d_1 x + d_2 x^2$ and $V \approx v_o + v_1 x$. Note that $d_o = 0$ because $\mathfrak{D} \sim A \sim x$ and that $v_o = 0$ if $G = 0$. We can then determine the indicial equation [8] of eq. (3.41) by using the ansatz $rE_\perp \sim x^\alpha$ in eq. (3.41). The coefficient of the lowest order in x yields the indicial equation, $d_1\alpha^2 = 0$, i.e. $\alpha = 0$ if $d_1 \neq 0$ (we exclude the case $d_1 = 0$). We now know that the two independent solutions of eq. (3.41) have the form [8] :

$$rE_\perp = \begin{cases} w_1(x) \quad \text{regular} \\ \\ w_2(x) = w_1(x)\log x + g(x),\ g(x) \text{ regular} \end{cases} \qquad (3.42)$$

For the subsequent discussion we need the form of $w_1(x)$. From (3.41) we can determine its expansion coefficients
$w_1(x) \approx c_o + c_1 x + c_2 x^2$:

$$\left.\begin{aligned} c_0 &= 1 \qquad \text{or arbitrary}, \\ c_1 &= -v_0/d_1, \\ c_2 &= -\frac{v_1}{4d_1} + \frac{v_0}{4d_1^2}(v_0 + 2d_2). \end{aligned}\right\} \tag{3.43}$$

An important result is, as we shall see, that $c_1 = 0$ if $G = 0$.

We can now determine the behaviour of the other field components in the neighborhood of the singularity, $x = 0$. From eq. (3.34) we obtain

$$i\frac{\omega}{c}B_{\parallel} = \mathcal{D}\frac{d}{dx}rE_{\perp} - \frac{k_{\perp}G}{(A-k_{\perp}^2)r}rE_{\perp} . \tag{3.44}$$

Since $k_{\perp}G/(A-k_{\perp}^2)r$ is in general finite at $x = 0$ we obtain that

$$B_{\parallel} \sim \log x \tag{3.45}$$

if $G \neq 0$ and $B_{\parallel} \sim (x^2 \log x + \text{regular})$ if $G = 0$. This difference in the singular behaviour of $B_{\parallel}$ was the main point we remarked [21] in comparing our cylindrical model with the slab model, eq. (3.39), or cylindrical models which did not include the equilibrium-current term.

Passing onto the remaining field components E_r, B_r and $B_{\perp}$, we find from Faraday's law, eq. (3.27), using eq. (3.25)

$$\frac{i\omega}{c}B_r = -ik_{\parallel}E_{\perp} \sim \log x , \tag{3.46}$$

$$i(A-k_{\perp}^2)rE_r = G(rE_{\perp}) - k_{\perp}(rE_{\perp})' \sim 1/x , \tag{3.47}$$

$$\frac{i\omega}{c}B_{\perp} = ik_{\parallel}E_r + \left(\frac{1}{r}\frac{B_{0\theta}}{B_0}\right)'rE_{\perp} \sim 1/x . \tag{3.48}$$

Hence the wave field near the singularity is dominated by the two components E_r and $B_\perp \sim (ck_\parallel/\omega)E_r$.

If, in the long run, we intend to calculate the resonantly-absorbed energy as we have learned to do it in the laser case, section 2.3, we will need the energy density, U, of the Alfvén oscillations in the neighborhood of the singularity. In general terms

$$U = \frac{1}{16\pi}\left[\vec{B}^*\cdot\vec{B} + \vec{E}^*\cdot\frac{\partial}{\partial\omega}(\omega\vec{\epsilon})\cdot\vec{E}\right], \qquad (3.49)$$

which around the singularity ($B_\perp$ and E_r dominant) reduces to :

$$U = \frac{1}{16\pi}|E_r|^2\left[\frac{c^2k_\parallel^2}{\omega^2} + \frac{\partial}{\partial\omega}(\omega\epsilon_{rr})\right]. \qquad (3.49')$$

Using eq. (3.30) for ε_{rr} one has

$$U = \frac{1}{8\pi}|E_r|^2\left[1 + \frac{c^2}{v_A^2}\sum_i \frac{f_i}{\left(1-\frac{\omega^2}{\omega_{ci}^2}\right)^2}\right]. \qquad (3.50)$$

Let us make a last remark on the singularity. By using eq. (3.34) in eq. (3.47) in order to eliminate $(rE_\perp)'$ one obtains the suggestive result

$$E_r = -i\frac{G}{A}E_\perp - \frac{k_\perp}{A}\frac{\omega}{c}B_\parallel, \qquad (3.51)$$

which corresponds to the eq. (2.25) of the laser case. If we were able to find a reasonable approximation for the driver, i.e., $E_\perp$ and $B_\parallel$ of the global oscillation of the plasma column, we could then use (3.51) to obtain the amplitude of the (damped) Alfvén-oscillation and hence the resonantly absorbed power, precisely as in the laser case. Note that $E_\perp$ can drive the Alfvén-oscillation only if $G \neq 0$.

4. WAVE EXCITATION

4.1 Exciting antenna

From now on we restrict ourselves to the case $v_A/c \ll 1$ and neglect the displacement current in Maxwell's equations. This excludes wave propagation in the vacuum surrounding the plasma and is a good approximation for AWH where usually the vacuum wavelength c/ω is larger than the system dimensions. For ICRF in large devices this approximation might be questionable. It facilitates, however, considerably the treatment of the vacuum field and the antenna problem.

We assume that the plasma of radius r_p is surrounded by vacuum and by an infinitely-conducting shell with radius r_s. Furthermore we assume that an antenna with radius r_a is situated in the vacuum region. The antenna is modelled as a mere layer of imposed currents and not as a piece of metal in which image currents could flow. Since we neglect displacement currents, the antenna currents must satisfy div $\vec{j} = 0$. In most of the published AWH work only infinitely-thin helical currents are used. Here we do a bit more by allowing for idealized radial feeders [27]. We can then model either pure helical antennae which do not need feeders to allow for div $\vec{j} = 0$ or pure poloidal antennae which do need feeders if $m \neq 0$.

To have an antenna model which satisfies automatically div $\vec{j} = 0$ we can argue as follows. The antenna current must have the form $\vec{j} = \mathrm{rot}\vec{b}$, where $\vec{b}$ is an arbitrary vector (which we could call the "current potential"). It depends on r and $\sim \exp i(m\theta+kz-\omega t)$. For the antennae we have in mind it is sufficient to have

$$\vec{b} = b_r\vec{e}_r + b_z\vec{e}_z, \tag{4.1}$$

and

$$\left.\begin{aligned} b_r &= -i(1-s)\delta(r-r_a)\beta, \\ b_z &= -ks\,\theta(r-r_a)\beta, \end{aligned}\right\} \tag{4.2}$$

where

$$\beta = \beta_o \exp i(m\theta+kz-\omega t). \qquad (4.3)$$

In the above, s ($0 \leq s \leq 1$) and β_o are real constants. As we shall see below β_o is related to the current flowing in an antenna "wire". The delta function, $\delta(r-r_a)$, defines the antenna sheet and the Heavyside function, $\theta(r-r_a) = \int \delta(r-r_a)dr$, defines the region of the radial feeders. This becomes clear when (4.1) - (4.3) are used to calculate the current $\vec{j} = \text{rot } \vec{B}$:

$$\left.\begin{aligned} j_r &= -is\,\frac{km}{r}\,\beta\,\theta(r-r_a), \\ j_\theta &= k\beta\,\delta(r-r_a), \\ j_z &= -(1-s)\,\frac{m}{r}\,\beta\,\delta(r-r_a). \end{aligned}\right\} \qquad (4.4)$$

We can now interpret the role of s : s = 0 is a helical antenna without feeders (Fig. 4.1), whereas s = 1 models an antenna which has poloidal currents in the sheet and these are fed by radial currents (Fig. 4.2). An antenna of finite extent as it is used in experiments (see Fig. 1.2) can be obtained as a Fourier-sum of antennae of the type of eq. (4.4). Particularly, a real antenna is "fixed in space": it has typically the dependence of a standing wave, e.g. sin (mθ+kz) sin ωt or even sin mθ sin kz sin ωt. Such antennae can also be obtained by superposition. For the time being we stick, however, to the "theoricians antenna" dependence ~ exp i(mθ+kz-ωt).

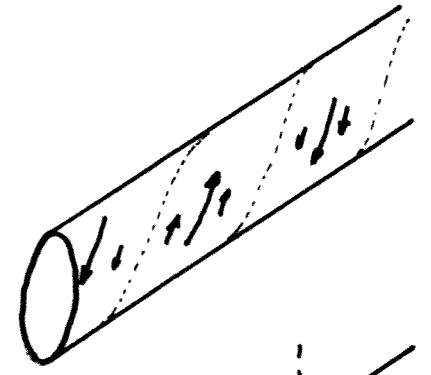

Fig. 4.1 Helical antenna (s = 0)

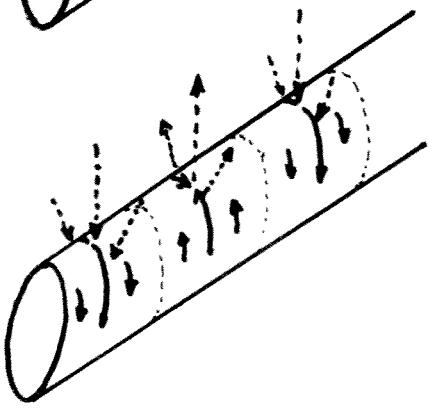

Fig. 4.2 Poloidal antenna with radial feeders (s = 1)

Let us calculate the current in a "wire", I, by which we mean the current flowing in a half period of exp i(mθ+kz−ωt). In Figs 4.1 and 4.2 this current is given by the current flowing in the helical or the poloidal strips, respectively. These strips are delimited by the dashed lines. Formally we can obtain it simply by integrating j_θ over half a period along z :

$$I = \int_{\text{half period}} \mathrm{Re}\, j_\theta \, dr dz = k\beta_0 \int \cos(m\theta + kz - \omega t)\, dz = 2\beta_0 . \qquad (4.5)$$

Our strip "wires" carry a current $2\beta_0$.

4.2 Vacuum wave equation

The surface-current-carrying sheet antenna can be treated as a discontinuity of the perturbed magnetic field in the vacuum. Its influence can be taken into account as a matching condition at $r = r_a$. This will be done in the next section. The radial current, however, is a volume current and has to be taken into account in the wave equation. The wave equation is

$$\mathrm{rot}\,\vec{B} = \frac{4\pi}{c} j_r \vec{e}_r \;, \quad r_p < r < r_a \quad \text{or} \quad r_a < r < r_s . \qquad (4.6)$$

Using $\mathrm{div}\,\vec{B} = 0$, eq. (4.6) and eq. (4.4) for j_r we obtain

$$\frac{1}{r}\frac{d}{dr} r \frac{dB_z}{dr} - \left(k^2 + \frac{m^2}{r^2}\right) B_z = \frac{4\pi}{c} \frac{m^2}{r^2} s k \beta\, \theta(r - r_a) . \qquad (4.7)$$

Once B_z is known, one can calculate the remaining components of $\vec{B}$:

$$\left.\begin{aligned} B_r &= -\frac{i}{k}\frac{dB_z}{dr} , \\ B_\theta &= \frac{m}{kr} B_z + \frac{i}{k}\frac{4\pi}{c} j_r . \end{aligned}\right\} \qquad (4.8)$$

The wave equation, eq. (4.7), is the equation of the modified Bessel function. It is inhomogeneous in the case of antennae with radial feeders. We could now solve this equation analytically. In general, this makes not much sense, since the eqs (3.34) and (3.35) anyway have

to be solved numerically for a realistic plasma. We then prefer to solve (4.7) numerically as well. Only the case of a homogeneous plasma without exciting antenna will be treated analytically (sect. 4.6).

4.3 Boundary conditions

4.3.1 Axis, r = 0

To specify fully our wave excitation problem we need, apart from the wave equations in the plasma and in the vacuum, the behaviour of the fields at the domain boundaries. Let us start with the axis r = 0 which is, as usual in cylindrical geometry, a singular point of the equations. For physical reasons the solutions have to be regular there. If we remember the discussion of eq. (3.36) we might realize that the solutions of eqs (3.34) and (3.35) must behave like

$$\left.\begin{aligned} rE_\perp &= r^{|m|}\,\mathcal{E}\,, \\ \frac{i\omega}{c}B_\parallel &= r^{|m|}\,\mathcal{B}\,, \end{aligned}\right\} \qquad (4.9)$$

where $\mathcal{E}(r=0)$ and $\mathcal{B}(r=0)$ are different from zero. The regularity condition is now a relation between these two quantities. It can be obtained by expansion around r = 0 : $\mathcal{E} = e_0 + e_1 r + \ldots$, $\mathcal{B} = b_0 + b_1 r + \ldots$, $G = g_0 + g_1 r + \ldots$, $A = a_0 + a_1 r + \ldots$, $k_\perp \approx m/r$. Inserting these expansions into eqs (3.34) and (3.35) we obtain to lowest order in r :

$$\left.\begin{aligned} (a_0|m| - m g_0)\,e_0 + m^2 b_0 &= 0\,, \\ (a_0^2 - g_0^2)\,e_0 + (a_0|m| + m g_0)\,b_0 &= 0\,. \end{aligned}\right\} \qquad (4.10)$$

First, we note that the determinant of eq. (4.10) is indeed zero allowing a non-vanishing solution for e_0 and b_0. The ansatz, eq. (4.9), is therefore correct. Second, we obtain the regularity condition :

$$\mathcal{E}(r=0) = \frac{m^2}{m g_0 - |m| a_0}\,\mathcal{B}(r=0)\,. \qquad (4.11)$$

Note that $\mathcal{E}(r = 0) = 0$ if $m = 0$ as we have found from eq. (3.36).

4.3.2 Plasma-vacuum interface, $r = r_p$

In contrast to MHD, the boundary conditions at $r = r_p$ in the present cold-plasma theory are trivial. We simply require the fields be continuous. By means of eqs (4.8) and (3.24) we obtain

$$B_{\parallel}(r_p - 0) = B_{\parallel}(r_p + 0) = \frac{\vec{B}_0}{B_0} \cdot \vec{B} = \frac{k_{\parallel}}{k} B_z(r_p + 0) . \qquad (4.12)$$

Furthermore, from $i\,\omega/c\, B_r = \mathrm{rot}_r \vec{E} = -ik_{\parallel} E_{\perp}$ and eq. (4.8)

$$E_{\perp}(r_p - 0) = -\frac{\omega}{ck_{\parallel}} B_r(r_p - 0) = -\frac{\omega}{ck_{\parallel}} B_r(r_p + 0) = \frac{i\omega}{ckk_{\parallel}} \left.\frac{dB_z}{dr}\right|_{r_p + 0} . \qquad (4.13)$$

4.3.3 Antenna, $r = r_a$

As at the plasma surface we need two matching conditions here. The first one is trivial and follows from $\mathrm{div}\, \vec{B} = 0$, namely $B_r(r_a - 0) = B_r(r_a + 0)$, or from eq. (4.8)

$$\left.\frac{dB_z}{dr}\right|_{r_a - 0} = \left.\frac{dB_z}{dr}\right|_{r_a + 0} . \qquad (4.14)$$

The second condition is for the tangential components of $\vec{B}$ which make a jump due to the surface current in the antenna sheet. It is sufficient to calculate the jump of B_z; that of B_θ follows automatically from eq. (4.8). We use Stokes' integral theorem for $\mathrm{rot}\, \vec{B} = (4\pi/c)\vec{j}$ with $\vec{j}$ given by eq. (4.4) :

$$\oint_{\delta D} \vec{B} \cdot d\vec{s} = \frac{4\pi}{c} \int\int_{D} \vec{j} \cdot d\vec{\sigma} . \qquad (4.15)$$

The proper choice of the domain D is shown in Fig. 4.3. If we choose $\Delta r \ll \Delta z$ the integral on the left-hand side is given by $[B_z(r_a+0) - B_z(r_a-0)]\Delta z$. The integral on the right-hand side is

$$-\Delta z \int_{r_a - \Delta r/2}^{r_a + \Delta r/2} j_\theta\, dr = -k\beta ,$$

and we obtain

$$B_z(r_a+0) = B_z(r_a-0) - \frac{4\pi}{c} k\beta \,. \tag{4.16}$$

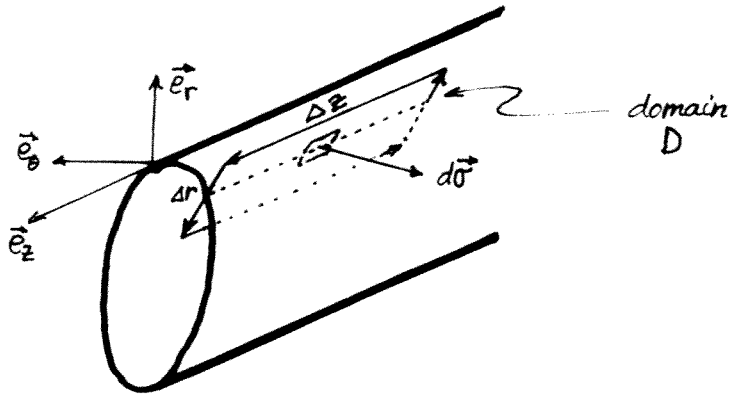

Fig. 4.3

4.3.4 Conducting shell, $r = r_s$

Since we assume infinite conductivity of the shell the tangential components of $\vec{E}$ must be zero, and therefore from
$i\,\omega/c\, B_r = \mathrm{rot}_r E = i\, m/r\, E_z - ikE_\theta = 0$ we have

$$\left.\frac{dB_z}{dr}\right|_{r_s} = 0. \tag{4.17}$$

4.4 Power emitted by the antennae

The power emitted by the antenna is

$$P = -\frac{1}{2}\int \vec{j}\cdot\vec{E}^*\, d^3r \,. \tag{4.18}$$

With this definition Re(P) describes the power (resonantly) absorbed by the plasma and Im(P) is the reactive power partly due to the vacuum magnetic field and partly due to the oscillating field and particle energy in the plasma. Instead of the total power P we prefer to work with the power emitted by a unit area of the antenna :

$$P/A = -\frac{1}{2r_a}\int \vec{j}\cdot\vec{E}^*\, r\, dr \,. \tag{4.19}$$

In our papers we have mostly used still another quantity, namely, the power per unit length of the machine $p = 2\pi r_a P/A$. Using the expressions for $\vec{j}$, eq. (4.4), we find

$$P/A = \frac{ms\beta}{2r_a}\int_{r_a}^{r_s} ikE_r^* dr - \frac{\beta}{2}\left(kE_\theta^* - \frac{m}{r_a}E_z^*\right)\Big|_{r_a} - \frac{s\beta}{2}\left(\frac{m}{r_a}E_z^*\right)\Big|_{r_a}.$$

With $i\,\omega/c\,\vec{B} = \mathrm{rot}\,\vec{E}$ and $E_z(r_s) = 0$ this yields

$$P/A = \frac{\beta}{2}\frac{\omega}{c}B_r^*\Big|_{r_a} + i\frac{s\beta}{2}\frac{m}{r_a}\int_{r_a}^{r_s}\frac{\omega}{c}B_\theta^* dr. \qquad (4.20)$$

Once we know the solution B_z and dB_z/dr we can calculate B_r^* and B_θ^* from eq. (4.8). There are several alternative forms of eq. (4.20) but in none have we been able to get rid of the integral term. There is one form which is useful for the estimation of the difference between a helical ($s = 0$) and a poloidal antenna with feeders ($s = 1$). This particular form is obtained when use is made of $\mathrm{div}\,\vec{B} = 0$ to eliminate B_θ^* from eq. (4.20)

$$P/A = (1-s)\frac{\beta}{2}\frac{\omega}{c}B_r^*\Big|_{r_a} - i\frac{s\beta}{2}\frac{k}{r_a}\int_{r_a}^{r_s}\frac{\omega}{c}B_z^* r dr. \qquad (4.21)$$

The power emitted by the poloidal antenna, $s = 1$, is entirely given by the integral term, in contrast to eq. (4.20). In eq. (4.21) we can use the wave equation, eq. (4.7), to find

$$P/A = (1-s)\frac{\beta\omega}{2c}B_r^*\Big|_{r_a} - s\frac{\beta\omega}{2c}\int_{r_a}^{r_s}\frac{k^2}{k^2+m^2/r^2}\frac{d}{dr}\left(\frac{r}{r_a}B_r^*\right)dr + \\ + is^2\frac{|\beta|^2}{2}\frac{4\pi\omega}{c^2}\frac{1}{r_a}\int_{r_a}^{r_s}\frac{k^2m^2}{k^2r^2+m^2}rdr. \qquad (4.22)$$

The first term is the power emitted by a helical ($s = 0$) antenna, the second term describes the resistive and a part of the reactive power emitted by a poloidal antenna. The third term is purely reactive and relevant to the poloidal antenna as well. From an inspection of the second term we learn that the resistive power has the same form for both antenna types, if $k \gg m/r_a$. In slab geometry, where $k \to k_z$, $m/r \to k_y$ and $r \to x$ the second term is integrable and yields

$$-s\frac{\beta\omega}{2c}\frac{k_z^2}{k_z^2+k_y^2}B_x^*\Big|_{x_a}. \qquad (4.23)$$

For a given B_x the power of a poloidal antenna is by a factor $k_z^2/(k_z^2 + k_y^2)$ smaller than that of a helical antenna. One can show that for a given current per "wire", I, the excitation of the plasma is smaller by the same factor. We have therefore

$$\text{slab}: \quad \frac{\mathrm{Re}\,(P/A)_{s=1}}{\mathrm{Re}\,(P/A)_{s=0}} = \left(\frac{k_z^2}{k_z^2 + k_y^2}\right)^2 . \qquad (4.24)$$

This relation is approximately true for the cylinder as we have found from numerical calculations [17],

$$\text{cylinder}: \quad \frac{\mathrm{Re}\,(P/A)_{s=1}}{\mathrm{Re}\,(P/A)_{s=0}} \approx \left(\frac{k^2}{k^2 + m^2/r_a^2}\right)^2 . \qquad (4.25)$$

A last remark concerning the power might be in order here. The wave equations in the plasma, eqs (3.34) and (3.35), can be written in real form if we take $i\,\omega/c\,B_\parallel$ to be real. If we take $i\beta \in \mathbb{R}$ then in the vacuum $iB_z \in \mathbb{R}$ as well as can be seen from eqs (4.7), (4.12), (4.13) and (4.16). We then find from eq. (4.8) that $B_r \in \mathbb{R}$ and the power, eq. (4.21), turns out to be purely imaginary, i.e. purely reactive. Remember that our model does not contain any dissipation as yet. All we have in eqs (3.34) and (3.35) are the singularities due to the Alfvén resonance, A = 0. The result "P/A imaginary" just tells us that we do not correctly evaluate these singularities by assuming all the quantities in eqs (3.34) and (3.35) to be real. Remember also that the Landau damping would vanish if we naively assumed the Landau contour going <u>through</u> the pole.

As in the Landau problem we can ensure causility by having $\omega + i\nu$ instead of ω, where $\nu > 0$ [28]. Alternatively, we can assume to have weak collisional damping (of the ions on neutrals, eq. (3.10)) which leads to the same result. From the treatment of the laser case (sect. 2.3) we know already that the absorption will not depend on the magnitude of ν.

4.5 Normalized quantities

From now on we will work with dimensionless quantities. Whether it is advantageous to do so or not is a question of taste. Within the present section we denote a quantity A in physical units by A and its normalized, dimensionless value by $\underset{\sim}{A}$. In the remainder of these lectures we shall work exclusively with the normalized quantities which then will be denoted by A again. Equations cited from the first part of the lectures will tacitely be taken in their normalized form. We use the following normalizations for length, time, mass density and the electromagnetic field :

$$\left.\begin{aligned} \underset{\sim}{r} &= r / r_p \,, \\ \underset{\sim}{t} &= t\, v_A(0) / r_p \,, \\ \underset{\sim}{\rho_0} &= \rho_0(r) \Big/ \sum_i n_{i0}(0)\, m_i \,, \\ \underset{\sim}{\vec{B}} &= \vec{B} / B_0(0) \,, \\ \underset{\sim}{\vec{E}} &= \vec{E}\, c / \left(v_A(0)\, B_0(0)\right) . \end{aligned}\right\} \qquad (4.26)$$

We stress the point again that <u>all</u> the quantities appearing in the remaining sections will have to be interpreted as dimensionless, for instance r_p has to be interpreted as $\underset{\sim}{r_p} = r_p/r_p = 1$ and ω_{ci} as

$$\underset{\sim}{\omega_{ci}} = \omega_{ci}\, r_a / v_A(0) \,. \qquad (4.27)$$

For a single species plasma $\underset{\sim}{\omega_{ci}}$ is, apart from the profiles of $\underset{\sim}{\rho_0}(r)$ and $\underset{\sim}{B_0}$ and the antenna structure and the shell $\underset{\sim}{r_a}$, $\underset{\sim}{r_s}$, m and k, the only free physical parameter

$$\underset{\sim}{\omega_{ci}} = \sqrt{4\pi}\,\frac{e}{c}\, r_p \sqrt{\frac{n_{i0} z^2}{m_i}} = 4.4 \times 10^{-8}\, r_p(cm) \sqrt{\frac{n_{e0}(cm^{-3})\, z}{\mu}} \,. \qquad (4.28)$$

Here $\mu = m_i/m_{proton}$ and z is the charge state of the ions. For a small device of the size of TCA ($r_p \approx 17$ cm) $\underset{\sim}{\omega_{ci}} \approx 2$, for PLT $\underset{\sim}{\omega_{ci}} \approx 5$ and for JET $\underset{\sim}{\omega_{ci}} \approx 20$, respectively.

Let us rapidly go through our equations, starting at eqs (3.34), and see which changes have to be made in order to have them in dimensionless form. From (3.34) and (3.35) merely the velocity of light, c, has to be dropped, the coefficient A and G being normalized by r_p^2, eq. (3.32). Equation (3.37) does not need any change. From rot $\vec{B} = (4\pi/c)\vec{j}$ we learn that j should be normalized by

$$\underset{\sim}{\vec{J}} = r_p \frac{4\pi}{c} \frac{\vec{J}}{B_0(0)} \quad . \tag{4.29}$$

In eq. (3.40) the $4\pi/c$ has to be dropped then. As to the normalization of the energy density, eq. (3.49) one may opt for $\underset{\sim}{U} = U/(B_0^2(0)/4\pi)$ and has to carry explicitly a factor $(v_A(0)/c)^2$ in the electric field term or one incorporates it in the definition of $\vec{\epsilon}$. The energy conservation law takes then the form

$$\frac{\partial \underset{\sim}{U}}{\partial t} + \underset{\sim}{\mathrm{div}}\ \underset{\sim}{\vec{S}} + \underset{\sim}{\vec{j}} \cdot \underset{\sim}{\vec{E}} = 0 \tag{4.30}$$

where the Poynting vector is given by $\underset{\sim}{\vec{S}} = \underset{\sim}{\vec{E}} \times \underset{\sim}{\vec{B}}$. The normalization of the current β, eq. (4.5) is obtained from eqs (4.4), (4.5) and (4.29). Equations (4.7), (4.8), (4.16) and (4.22) loose their factors $4\pi/c$ and in eqs (4.9), (4.13), (4.20) - (4.23) c does not appear. The power per unit area P/A, eqs (4.19) - (4.25), has the same units as $\vec{S}$, i.e. $\underset{\sim}{(P/A)} = (P/A)\ 4\pi/(v_A(0)\ B_0(0)^2)$.

4.6 The eigenvalue problem in a homogeneous plasma

Before we describe the numerical treatment of the wave excitation problem (which is fully defined now) and the results for realistic plasmas it is advantageous for our understanding to discuss the eigenoscillations of a homogeneous plasma column. In the laser case we succeeded to draw a simple picture of the physics by describing separately the energy-carrier wave (the electromagnetic wave) and the energy-absorbing local oscillation (the electrostatic wave). For the present AWH or ICRF case we have discussed the absorbing oscillation so far (sect. 3.3). We now aim at a description of the energy-carrier, i.e. the global oscillation of the plasma column.

We assume all the equilibrium quantities to be constant and the equilibrium current to be zero. Under these assumptions the magnetic field is axial, $\vec{e}_{\parallel} = \vec{e}_z$, and the wave equation in the plasma is given by eq. (3.40)

$$\frac{1}{r}\frac{d}{dr}\, r\, \frac{dB_z}{dr} + \left(k_r^2 - \frac{m^2}{r^2}\right) B_z = 0, \tag{4.31}$$

where

$$k_r^2 = (A^2 - G^2)/A \,. \tag{4.32}$$

This is an ordinary Bessel equation if $k_r^2 > 0$ and the equation of the modified Bessel function if $k_r^2 < 0$ [7] :

$$B_z(r) = C_1 Z_m(|k_r| r) = \left\{ \begin{array}{l} C_1 J_m(|k_r| r) \text{ for } k_r^2 > 0 \\ C_1 I_m(|k_r| r) \text{ for } k_r^2 < 0 \end{array} \right\} \tag{4.33}$$

where C_1 is a constant. By excluding Y_m and K_m from our solution we have satisfied the regularity condition at the axis, eq. (4.11). Since we treat the eigenvalue problem, no antenna is situated in the vacuum $r_p < r < r_s$. The solution of the wave equation in the vacuum, eq. (4.7), is

$$B_z = C_2 I_m(kr) + C_3 K_m(kr) \,, \tag{4.34}$$

where C_2 and C_3 again are constants. By using the 3 remaining boundary conditions, eqs (4.12), (4.13) and (4.17), one can eliminate the 3 unknown constants C_1, C_2, C_3 and find the dispersion relation of the eigenoscillation. Equation (4.17) requires $dB_z/dr = 0$ at $r = r_s$, hence

$$C_2/C_3 = -D_m(kr_s), \qquad D_m(kr_s) \equiv K_m'(kr_s)/I_m'(kr_s) \,. \tag{4.35}$$

Here the prime denotes the derivative with respect to argument. Equation (4.12) requires B_z be continuous across $r = r_p = 1$, hence

$$C_3/C_1 = Z_m(|k_r|)/\left(-D_m(kr_s) I_m(k) + K_m(k)\right) \,. \tag{4.36}$$

By means of eq. (3.35) the last matching condition, eq. (4.13), can be written as

$$-\frac{k_r^2}{k^2}\left.\frac{dB_z}{dr}\right|_{r_p+0} = \left.\frac{dB_z}{dr}\right|_{r_p-0} + m\frac{G}{A}B_z(r_p-0)\,, \tag{4.37}$$

and yields the dispersion relation

$$\frac{Z_m'(|k_r|)}{Z_m(|k_r|)} + \frac{m}{|k_r|}\frac{G}{A} + \mathrm{sign}(k_r^2)\frac{|k_r|}{k}F_m(k,r_s) = 0\,, \tag{4.38}$$

where

$$F_m(k,r_s) = \frac{D_m(kr_s)I_m'(k) - K_m'(k)}{D_m(kr_s)I_m(k) - K_m(k)}\,. \tag{4.39}$$

For the discussion of (4.38) we restrict ourselves to the case of a single species plasma and we closely follow Ref. 29. We cannot just copy Ref. 29 because the analytical relations derived there hold only for $m = \pm 1$, which unfortunately was forgotten when the text was written.

It is easy to solve eq. (4.38) numerically. A numerical solution is shown in Fig. 4.4. The free parameters are taken to be $\omega_{ci} = 2$ and $r_s = 1.5$ which are typical values of the TCA tokamak [14]. The eigenfrequencies $x = \omega/\omega_{ci}$ are shown for $m = +1$ and $m = -1$ as a function of k.

It is possible to obtain analytical solutions of eq. (4.38) in the limit $k \ll 1$. We note that for $x \ll 1$ $I_0(x) \sim 1$, $I'_0(x) \sim x/2$, $K_0(x) \sim -\log x$, $K'_0(x) \sim -1/x$, $I_m(x) \sim x^\nu/(2^\nu \nu!)$, where $\nu = |m| \neq 0$, $I'_m(x) \sim I_m(x)\,\nu/x$, $K_m(x) \sim (\nu-1)!\,2^{\nu-1}/x^\nu$ and $K'_m(x) \sim -K_m(x)\,\nu/x$. It follows that $D_0(kr_s) \sim -2/k^2r_s^2$ and $D_m(kr_s) \sim \nu!(\nu-1)!\,2^{2\nu-1}/(k^{2\nu}r_s^{2\nu})$. All this combined yields

$$F_m(k,r_s) = \begin{cases} \dfrac{k}{2}\left(r_s^2-1\right) & m = 0 \\ -\dfrac{\nu}{k}\dfrac{r_s^{2\nu}-1}{r_s^{2\nu}+1} & \nu = |m| = 1,2,3,\ldots \end{cases} \tag{4.40}$$

Apart from the case m = 0, there are two possibilities to satisfy eq. (4.38) at $k \ll 1$. The first possibility (which is missing for m = 0) is to have $k_r \sim k$. Because $Z_m'(|k_r|)/Z_m(|k_r|) \sim 1/|k_r|$ all three terms in eq. (4.38) are of order 1/k and it is possible to satisfy the equation. If, on the contrary, $k_r > 1$, then either $A \sim k^2$ or $Z_m(|k_r|) \sim k^2$, i.e. $|k_r|$ is near to a zero of Z_m.

Let us first discuss the last case. The function Z_m must be the ordinary Bessel function J_m and $k_r^2 > 0$. From eq. (3.32) we have

$$A = \omega_{ci}^2 \frac{x^2}{1 - x^2} - k^2 ,$$
$$G = \omega_{ci}^2 \frac{x^3}{1 - x^2} . \qquad (4.41)$$

In order to have $k_r^2 \gtrsim 1$ we need $|x| \sim 1$ and therefore can neglect k^2 in eq. (4.41) with the result

$$k_r^2 = \omega_{ci}^2 x^2 = \omega^2 . \qquad (4.42)$$

For the case shown in Fig. 4.4 $\omega = j_{1,s}$, s = 1, 2, ..., where $j_{1,s}$ denotes the zeros of J_1. These are the frequencies of the radial eigenmodes of the fast magnetosonic wave (F) as they are known from ideal MHD [30]. The first zero, $j_{1,1} = 3.83$, leads to $x = \omega/\omega_{ci} = 3.83/2 = 1.91$. In Fig. 4.4 this mode is denoted with F_2 as the second radial eigenmode of the fast wave. As long as $k \lesssim 1$ this mode and all the higher ones are practically identical for m = ± 1.

The first radial eigenmodes of the fast wave F_1 are obtained in the limit $k_r \sim k \to 0$. After expansion of the function Z_m, i.e., $J_m'/J_m \sim |m|/|k_r|$ the dispersion relation (4.38) becomes

$$1 + \frac{\sigma G}{A} - \frac{k_r^2}{k^2} Q = 0 , \qquad (4.43)$$

where σ = sign (m) and $Q = (r_s^{2m} - 1)/(r_s^{2m} + 1)$. Using the definition of k_r^2, eq. (4.32), we find

$$A - \sigma G = k^2/Q. \qquad (4.44)$$

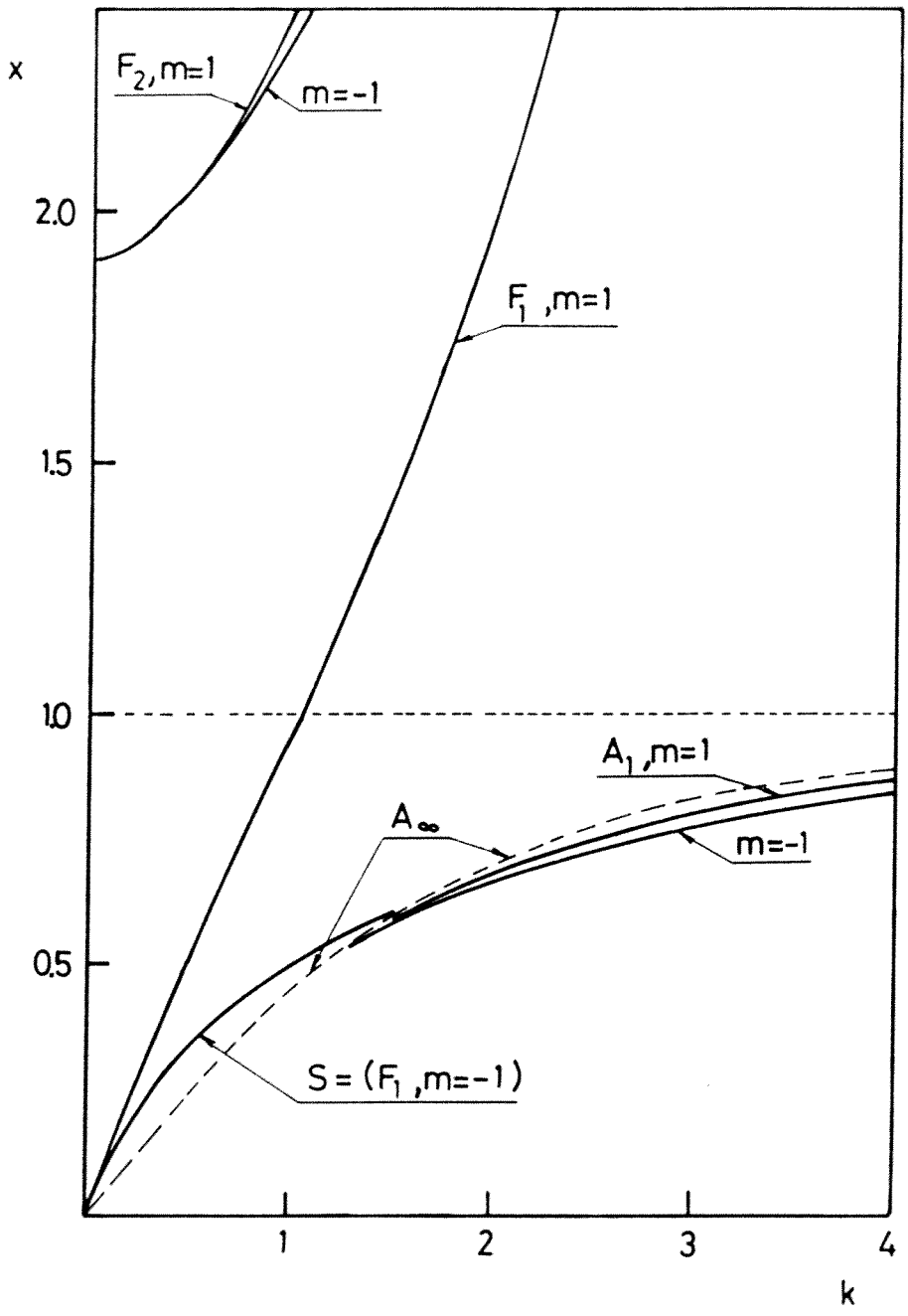

Fig. 4.4

Using eqs (4.41) for A and G we obtain a quadratic equation for ω/ω_{ci} whose positive-frequency solution is

$$\omega/\omega_{ci} = x = \alpha \left(1 + \mathrm{sign}(m)\, \alpha/2 \right), \qquad (4.45)$$

where

$$\alpha^2 = \frac{k^2}{\omega_{ci}^2} \left[1 + \frac{r_s^{2m} + 1}{r_s^{2m} - 1} \right]. \qquad (4.46)$$

Equations (4.40) and (4.46) hold even for $kr_s \to \infty$ and $k \to 0$ as can be shown by expanding D_m, eq. (4.35), $D_m(kr_s) \sim - \pi \exp(-2\, kr_s)$. If we take this limit in eqs (4.45) and (4.46) we find $\omega = \sqrt{2}\, k$. This is the surface eigenmode frequency as given by ideal MHD theory [31]. In an MHD treatment (i.e. $\omega_{ci} \to \infty$) the two modes for $m = \pm 1$ behave identically and like an eigenmode of the fast wave. It seems therefore natural to identify the first radial eigenmode of the fast magnetosonic wave F_1 with the surface eigenmode S.

In Fig. 4.4 only the mode F_1, $m = -1$ has been labelled with S for the following reason. For small k the wave fields of F_1 are global functions as opposed to those of the surface wave in plane geometry where they are confined to the neighborhood of the plasma-vacuum interface. It is only for $k \gtrsim 1$ that the mode F_1, $m = -1$ has surface-wave character as can be seen from Fig. 4.5. The mode F_1, $m = 1$ has global wave fields for all values of k. The surface-wave character of F_1, $m = -1$ in cylindrial geometry is clearly related ot the fact that it merges with the Alfvén resonance $A = 0$, denoted by A_∞ (at $k = 1.5$ in the case of Fig. 4.4). The value of k where S and A_∞ merge depends on r_s as we shall see in Fig. 4.6.

Let us, however, first finish the discussion of Fig. 4.4 by describing the global eigenmodes of the Alfvén wave (GEAW). These modes have often been called ion-cyclotron modes and very recently "discrete Alfvén waves" [15]. For small k they correspond to the combination $A \sim k^2$, $k_r > 1$ satisfying eq. (4.38). As can be seen from Fig. 4.4 there is no physical interest to obtain solutions for $k \ll 1$ because the whole class is extremely densely packed; in the MHD limit the solutions are even infinitely degenerate. For $k > 1.5$ the eigenfrequencies of the lowest radial modes (only A_1, $m = \pm 1$ are shown; all the higher modes,

A_S, $s > 1$, lie between A_1 and A_∞) are distinctly detached from the accumulation point A_∞. In the case shown, $r_S = 1.5$, $\omega_{ci} = 2$, the largest distances have been found around $k \approx 3.5$. The relative distances $(\omega_\infty - \omega_S)/\omega_\infty$ are 7.2 %, 3.2 % and 1.7 % for the modes $s = 1$, 2, 3, $m = -1$ and 3.6 %, 1.8 %, 1.1 % for $m = 1$. It is interesting to note, that the set of A_S, $m = -1$ seems to contain one mode more than $m = 1$, namely the mode A_1. All the other modes can, in fact, be put into a close one-to-one correspondance, $A_{S+1}(m = -1) \approx A_S(m = 1)$, with respect to frequency and radial wavenumber k_r (not shown). At small k the surface mode S has been identified as an eigenmode of the fast wave; at high k it now appears as a part of the Alfvén wave. This is, however, from a purist's point of view, somewhat misleading. Strictly speaking, the mode lies always <u>above</u> A_∞ and should therefore not be identified with any eigenmode of the Alfvén wave.

A detailed investigation of the behaviour of the surface mode as a function of k and of the radius of the conducting shell, r_S, has been made. The most striking result is shown in the upper part of Fig. 4.6. The radial wavelength k_r changes from real to imaginary as k grows. This fact explains the change (Fig. 4.5) form a global wave form at $k = 0.4$ to the surface wave form at $k = 1.5$: at $k = 0.4$ the eigenfunction for $B_\parallel$ is given by $J_1(\sqrt{.15}\ r)$ whereas at $k = 1.5$ $B_\parallel$ is given by an exponentially growing I_1 $(|k_r|\ r)$. We note the strong effect of the conducting shell. The smaller the vacuum gap the higher are the axial phase velocities ω/k at small values of k (see lower part of Fig. 4.6). This fact is well described by eq. (4.45) which for $k \lesssim 0.4$ approximates the exact result within 10 %. From eq. (4.45) we conclude that the phase velocities of the mode F_1, $m = 1$ show the same tendency to increase, when the shell is approached to the plasma, as those of the surface wave. This effect has been described by Paoloni [32].

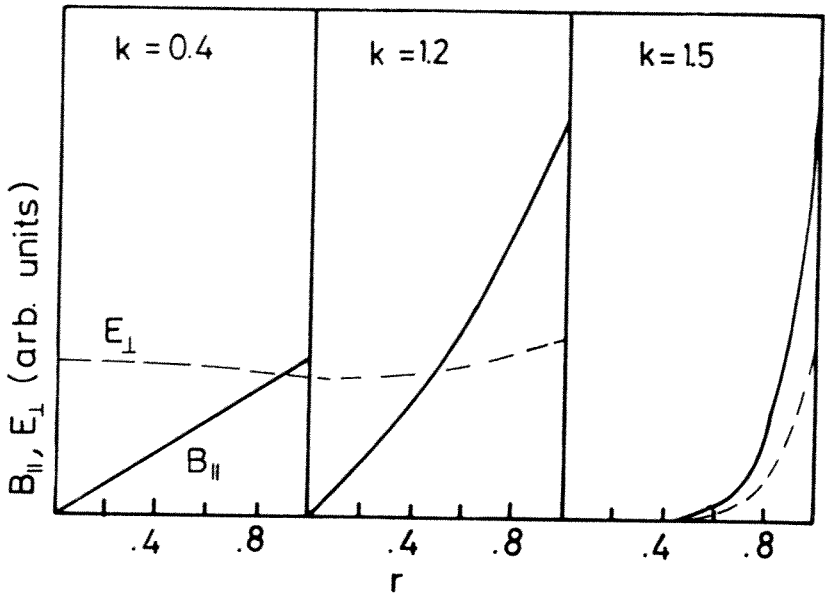

Fig. 4.5

4.7 The role of the global modes

In our organ-pipe picture (in contrast to WKB) of AWH it is the global modes which can be excited by the antenna. We call them "global modes" because their excitation engenders an overall field in the plasma and the vacuum. Conversely, they can be excited by a perturbation of the vacuum field, i.e. by an external antenna. In contrast, local modes cannot or only with difficulty be excited by an external antenna. By local modes we mean either the singular perturbations around r_o, $A(r_o) = 0$, in an inhomogeneous plasma or local perturbations in a homogeneous plasma as they can be obtained from a superposition of global eigenmodes of the Alfvén waves A_s, with high radial mode numbers s.

Since the local modes satisfy $A(r_o) \approx 0$, the frequency depends merely on $k_\parallel$ and, as a consequence, their group velocity perpendicular to the field is approximately zero. They cannot, therefore, transport energy from the plasma boundary to the interior. This role has to be played by the global modes. Candidates are all the eigenmodes, F_s, of the fast wave and the low-s eigenmodes, A_s, of the Alfvén wave.

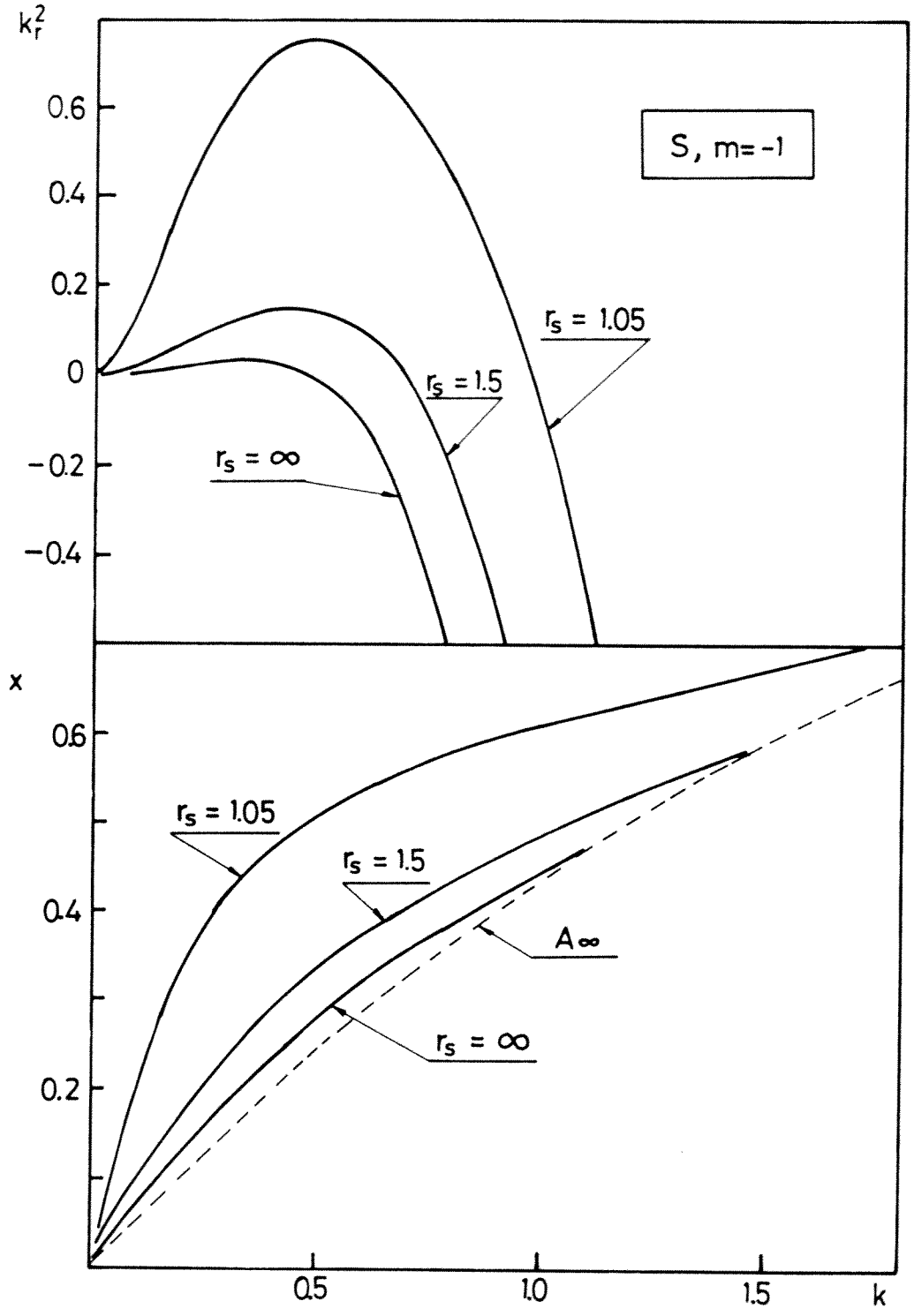
k_r^2
0.6
0.4
0.2
0
-0.2
-0.4
S, m=-1
r_s = 1.05
r_s = 1.5
r_s = ∞
x
0.6
0.4
0.2
r_s = 1.05
r_s = 1.5
A∞
r_s = ∞
0.5
1.0
1.5
k

Fig. 4.6

If we ignore, for the time being, the phenomenon of resonant absorption in an inhomogeneous plasma we can envisage to heat a plasma by exciting a global mode. Collisional damping (resistivity, viscosity) or Landau damping would transform its energy into heat. Such a heating scheme suffers from the weakness of the mentioned damping processes which makes the resonance (global resonance !) of the mode extremely sharp (high-Q "cavity" mode). Values of the order of 10^{-2} - 10^{-4} for $\Delta\omega/\omega$ [33] are not unusual. This fact leads to a technical problem : the frequency of the RF-generator has to follow (to track) the eigenfrequency of the global mode as the plasma parameters evolve during the heating pulse.

Heating by excitation of eigenmodes of the fast wave (and maybe of the Alfvén wave) has been observed in many ICRF-experiments. The eigenmodes manifest themselves by spikes in the loading impedance of the antenna, Re P/A, eq. (4.19), as the plasma parameters evolve. Spikes which are definitely due to resonances with eigenmodes of the Alfvén wave (A_1,A_2) have been observed in the TCA tokamak [14,15].

Coming back to resonant absorption now, we must realize that an inhomogeneous density of the form, say, $n_o = 1 - r^2$, fills the space between the lines A_∞ and $x = \omega/\omega_{ci} = 1$, Fig. 4.4, with the Alfvén continuum. This means that with (k,ω) falling between those two lines a field perturbation has a singularity at $r = r_o$ where $A(r_o) = 0$. The modes F_1 and S in Fig. 4.4 hence are coupled to the singular modes. They can resonantly loose their energy at the singularity.

As long as the equilibrium current is not introduced into the picture a pair (ω,k) lying near to A_∞ corresponds to a point r_o near to center. Conversely, a pair (ω,k) nearer to $\omega/\omega_{ci}=1$ corresponds to a resonance near the plasma boundary. Since the aim of a heating scheme must be to deposit the energy as near as possible to the centre of the plasma, the surface mode S must clearly be the best candidate for AWH.

In large devices ω_{ci} is, however, a large number and several eigenmodes, F_S, of the fast wave fall into the region below ω/ω_{ci} = 1, Fig. 4.7. Under such conditions it could be envisaged to use the lowest-s modes with quite good penetration features. A detailed comparison between F1(S) and F2 has been made in Ref. 17.

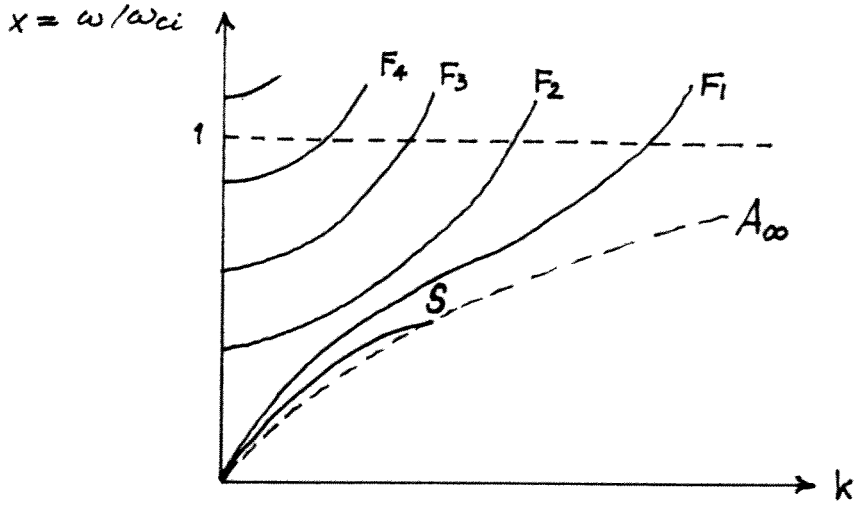

Fig. 4.7

In a two-species plasma with $\omega_{c1} < \omega_{c2}$ there are two continua, one lying between $A_{\infty 1}$ and $\omega = \omega_{c1}$ and the other lying between $A_{\infty 2}$ and $\omega = \omega_{c2}$. Each continuum has an associated surface mode and global eigenmodes of the Alfvén wave [34].

Conventionally one could call the lower continuum the Alfvén continuum and the higher one the "ion-ion hybrid" continuum (used in the ICRF mode-conversion scenario). Both, however, have the same origin and both species contribute to the physics in both continua.

We have now a clear picture of both, AWH and the ICRF mode-conversion scenario. The antenna excites a global mode which transports the energy to the singularity where it is resonantly absorbed in the cold-plasma picture and linearly converted into a short-wavelength mode in the warm-plasma pictures. At this point we could use the knowledge of the waveform of the global mode as obtained for a homogeneous plasma in the previous section (sect. 4.6) for an absorption calculation relevant to an inhomogeneous plasma and based on eqs (3.50) and (3.51). One would, as in the laser-case, sect. 2.3, assume that the collisional power loss is given by νU, eq. (3.50), with $\omega \to \omega + i\nu$. Also, one would assume that the wave structure of the global mode of the homogeneous cylinder is representative of the regular part of the wave structure in the inhomogeneous plasma cylinder. It is to be expected that such a procedure could produce reasonably good results for AWH where S is used as global mode. It is not clear whether ICRF, which tends to use higher F_S-modes, could be modelled in this way. A precise evaluation of the antenna-loading impedance in both cases can only be performed with numerical means.

5. NUMERICAL METHODS

5.1 Shooting method

Certain types of one-dimensional (1D) inhomogeneous boundary-value problems can be solved by the shooting method. It consists, as its name indicates, in solving the boundary-value problem as an initial-value problem. One solves the corresponding differential equation (or equations) from, say, left to right in the problem domain and varies the initial conditions on the left boundary until the condition imposed on the right boundary are satisfied.

The method can be described in a different manner giving it a somewhat less heuristic aspect. Let us assume that our boundary-value problem is described by a system of two 2nd order ordinary differential equations with 2 boundary conditions imposed on both boundaries of the domain. What would an analytician do ? He would determine 4 linearly independant fundamental solutions of the system and superpose them with the appropriate coefficients determined by the boundary conditions as we have done it in sect. 4.6 for a second order equation in two adjacent domains. The same can be done on the computer with the only difference that we determine directly two fundamentals which satisfy the conditions on the left boundary. All we need to do is to combine them in such a way that they satisfy the conditions on the right boundary.

For a second order equation in a single domain or second order equations in adjacent domains the shooting method works well, is rapidly programmed (e.g. by using a Runge-Kutta integrator), and yields quite efficient codes which do not need much memory nor excessive CPU-time. It does not work for homogeneous boundary-value problems, i.e., eigenvalue problems, with a non-compact operator, i.e., operators which have a continuous frequency spectrum as our Alfvén problem with $\nu = 0$. The evident reason is that it is impossible to cross the singularity.

Another situation where a straightforward shooting method does not work is given by the kinetic problem of mode conversion because of the

appearance of the short-wavelength warm-plasma mode. The corresponding system of two 2nd order differential equations has 4 fundamentals of which two correspond to a left- and a right-running, damped, short-wavelength mode. The small-scale wave which propagates against the direction of integration is "generated" from numerical noise and appears as an exponentially growing solution (in the direction of integration). The unphysical, exponentially-growing part dominates the real physics and makes it disappear in the round-off error long before the integration procedure has reached the other end of the domain. Multiple shooting techniques where the domain is sliced up into subdomains are presently in development and should cure the problem created by the different length scales.

The above somewhat lengthy introduction to the shooting method is to be understood as an attempt to motivate the reader to study the next section where a different method with a wide application potential (eigenvalue problems, kinetics, 2D, etc.) is presented. Had we in AWH and ICRF to tackle only eqs (3.34) and (3.35) the shooting method would be good enough.

We now discuss briefly how the eqs (3.34) and (3.35) can be solved by the shooting method. One problem, typical to cylindrical geometry, is posed by the fundamental which is singular at the axis. We cannot integrate from the boundary towards the axis because under all circumstances we would pick up the singular solution as we approach the axis. We therefore have to start at, or at least very near to, the axis and exclude explicitly the singular solution, i.e., we impose the regularity condition, eq. (4.11). To be able to apply it, we use the variables $\mathcal{E}$ and $\mathcal{B}$, eq. (4.9), instead of $E_\perp$ and $B_\parallel$. Equations (3.34) and (3.35) written for these variables are :

$$\left.\begin{aligned} \frac{d\mathcal{E}}{dr} &= \left[\frac{Gk_\perp}{A} - \frac{|m|}{r}\right]\mathcal{E} + \frac{A-k_\perp^2}{A}\, r\,\mathcal{B}, \\ \frac{d\mathcal{B}}{dr} &= \frac{G^2-A^2}{Ar}\,\mathcal{E} - \left[\frac{Gk_\perp}{A} + \frac{|m|}{r}\right]\mathcal{B}. \end{aligned}\right\} \qquad (5.1)$$

Remember that ω has to be replaced by $\omega + i\nu$ in the expressions for A and G.

We start with the integration at $r = \delta \ll 1$ by choosing $\mathcal{E} = 1$ and $\mathcal{B}$ according to eq. (4.11). Once the boundary, $r_p = 1$, reached, we know $E_\perp\ (r_p-0)$ and $B_\parallel(r_p-0)$ up to a constant C_1. Now we use the matching conditions, eqs (4.12) and (4.13), and obtain $B_z(r_p+0)$ and $dB_z/dr\,|_{r_p+0}$ up to the same constant. Using eq. (4.7) we integrate the B_z up to the antenna where we obtain the numbers, say, b_1 and d_1, for B_z and dB_z/dr still affected by the constant C_1, i.e.,

$$B_z(r_a-0) = C_1 b_1\,, \quad dB_z/dr\big|_{r_a-0} = C_1 d_1\,. \tag{5.2}$$

In a second step we integrate eq. (4.7) from r_s towards r_a. As initial conditions at $r = r_s$ we choose $B_z = 1$ and $dB_z/dr = 0$. The latter satisfies the boundary condition, eq. (4.17). Arriving at r_a+0 we find the numbers b_2 and d_2 for B_z and dB_z/dr which this time are affected by another free constant, C_2, i.e.,

$$B_z(r_a+0) = C_2 b_2\,, \quad dB_z/dr\big|_{r_a+0} = C_2 d_2\,. \tag{5.3}$$

In other words, we have found the values b_1, d_1, b_2 and d_2 of the fundamental solutions at the antenna satisfying all the boundary and matching conditions apart from those at the antenna. The free constants C_1 and C_2 have now to be chosen in such way that eqs (4.14) and (4.16) are also satisfied. We find

$$\left.\begin{aligned} C_1 &= \frac{d_2}{d_1}\, C_2\,, \\ C_2 &= -k\beta \,/\, \Big(b_2 - \frac{d_2}{d_1}\, b_1\Big)\,. \end{aligned}\right\} \tag{5.4}$$

Once the field B_z is known all the other fields can be calculated, in particular the antenna-loading or the power, eq. (4.20), can be obtained.

One remark is in order here. One can use the same procedure to determine eigenmodes and eigenfrequencies of the system as long as one

has no singularity in the plasma. In this case the antenna current β is zero, and we have to match the solutions continuously across r_a. The condition for this is

$$b_1 / d_1 = b_2 / d_2 \quad . \tag{5.5}$$

If this condition is satisfied for a given ω, we have found an eigenfrequency and an eigenfunction. In general the eigenfrequencies can be complex. In the ideal MHD model the eigenfrequencies of instabilities are purely imaginary, i.e., $\omega^2 \in \mathbb{R}$.

5.2 Variational methods

5.2.1 The weak variational form of the boundary-value problem

There is a powerful numerical-discretization procedure which, in our opinion, particularly suits theoreticians : the finite-element method. Usually this method is not applied directly to the pertinent differential equation but to its weak or Galerkin variational form. Here we shall present only the very essence of the procedure. For mathematical details the reader is referred to text books such as Ref. 35.

The method is applicable to multi-dimensional boundary value problems in complex domains. In fact, it has been invented by structural engineers. For the presentation of the basic ideas it is, however, sufficient to go through a simple example. We choose a 1D inhomogeneous boundary-value problem which is described by a 2nd order differential equation, a problem which could be solved by the shooting method as well.

Let our model equation be

$$u'' + p(x)\,u' + q(x)\,u = s(x), \tag{5.6}$$

subject to the boundary conditions, say,

$$u(0) = 0,$$
$$u'(1) = 1. \qquad (5.7)$$

The prime denotes the derivative d/dx and p(x), q(x) and s(x) are given funtions of x of sufficient regularity. Let v(x) be a test-function in some functional space of sufficient regularity (v' must exist), then

$$-\int_0^1 v'u'dx + v(1)u'(1) - v(0)u'(0) + \int_0^1 v(pu' + qu)dx = \int_0^1 vs\,dx. \qquad (5.8)$$

The natural boundary condition, u'(1)=1, can be used directly in eq. (5.8). The essential condition, u(0)=0, however, has to be imposed on the functional spaces of u(x) and v(x) explicitly, i.e., u(0)=v(0)=0. With this, eq. (5.8) becomes

$$-\int_0^1 v'u'\,dx + \int_0^1 vpu'dx + \int_0^1 vqu\,dx = \int_0^1 vs\,dx - v(1)\,. \qquad (5.9)$$

Eq. (5.9) is called the weak variational form of eqs (5.6) and (5.7) and is equivalent to them under the essential condition u(0)=v(0)=0. Equation (5.9) becomes a usual (strong) variational form if p(x)=0. Interestingly, in eq. (5.9) only the first derivatives must exist (they do not need to be continuous) in contrast to eq. (5.6). For the precise mathematics see Ref. 35.

For numerical purposes one approximates eq. (5.9) in a suitable manner. We shall discuss merely the finite-element method and merely in its simplest form.

5.2.2 Finite elements

The basic idea consists in dividing the domain $0 \leq x \leq 1$ into a finite number of, in general, unequally sized subdomains (the finite elements), $0 = x_0 < x_1 < \ldots < x_{n-1} < x_n = 1$, approximating the functions u(x) and v(x) by simple functions in each subdomain.

For the problem at hand it is sufficient to approximate the functions by linear functions, Fig. 5.1. As a rule of thumb one can say

that the simplest functions having the required regularity properties are the best for numerical purposes. To choose linear functions is sufficient in our case because the integrals in eq. (5.9) exist if u, u', v and v' exist. It does not matter that the derivatives u' and v' are discontinuous.

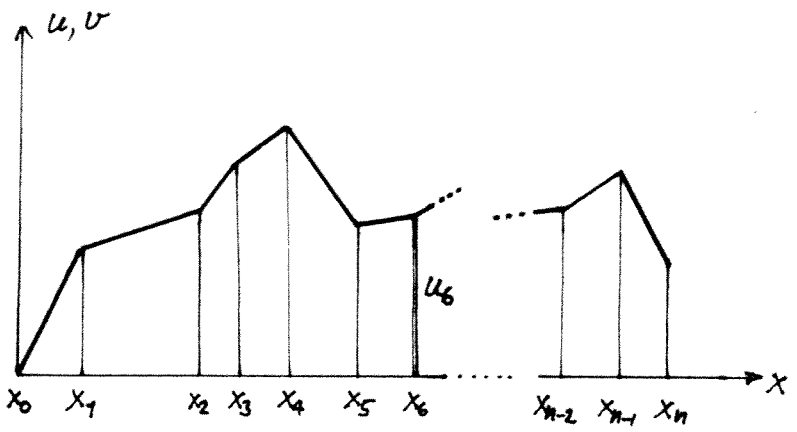

Fig. 5.1

The method losses its somewhat heuristic touch, once the basis functions of the finite-dimensional function spaces of u and v are introduced. By the way, u and v do not have to belong to the same space as they do in our example. The basis functions, $\psi_i(x)$, which allow us to describe a function of the type shown in Fig. 5.1 are defined by

$$\psi_i(x) = \begin{cases} 0 & x \leq x_{i-1} \\ \dfrac{x - x_{i-1}}{x_i - x_{i-1}} & x_{i-1} \leq x \leq x_i \\ \dfrac{x_{i+1} - x}{x_{i+1} - x_i} & x_i \leq x \leq x_{i+1} \\ 0 & x_{i+1} \leq x \end{cases} \tag{5.10}$$

The function $\psi_i(x)$ is shown in Fig. 5.2. A function u(x) is defined by its values u_j, Fig. 5.1, at the mesh points. Formally we have

$$u(x) = \sum_{j=1}^{n} u_j \psi_j(x) . \tag{5.11}$$

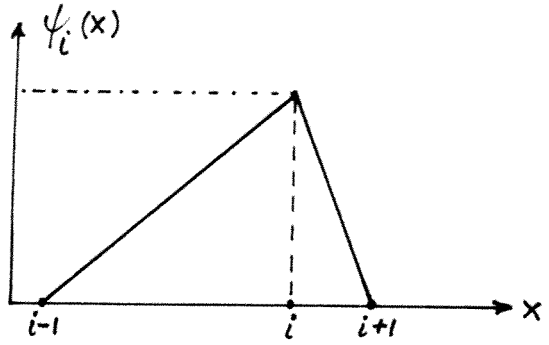

Fig. 5.2

Note that we have chosen the functional space such that u(0) = 0 by starting the sum at j = 1 and not at j = 0. We can construct from eq. (5.9) n linearly independent equations for the n unknowns u_j by choosing turn by turn $\psi_1(x)$, $\psi_2(x)$,...$\psi_n(x)$ as test functions; in loose words, by projecting the discretized version of eq. (5.6) (forgetting about the nonexistence of d^2u/dx^2) onto the basis, ψ_i, i = 1, ..., n :

$$\sum_j \left[-\int_0^1 \psi_i' \psi_j' dx + \int_0^1 \psi_i p \psi_j' dx + \int_0^1 \psi_i q \psi_j dx \right] u_j = \int_0^1 \psi_i s\, dx - \delta_{in} \quad , \quad i = 1, \ldots, n \tag{5.12}$$

The matrix A_{ij}, given by the square bracket in eq. (5.12), is tridiagonal because

$$\int \psi_i \psi_j \, dx = 0 \quad \text{if} \quad |i-j| \geq 2 \, . \tag{5.13}$$

The basis is almost orthogonal. It is very easy to solve a linear system for u_j

$$\sum_j A_{ij} u_j = r_i \, , \qquad i = 1, \ldots, n \tag{5.14}$$

by Gauss elimination when the coefficient matrix A_{ij} has a band-width of 3. In 2D problems, which are discretized in the same spirit, the band-width is proportional to the number of mesh points in one direction. Iterative solution techniques might then be more efficient. They would certainly need less memory.

5.3 Numerical problems associated with presence of continuous spectra [10]

Since the paper published on this subject [10] is written in quite simple terms it is not worthwhile to repeat the arguments here. We can read it without going back to the references cited. There is only one concept which we have not encountered in the course of these lectures, the concept of "spectral pollution". To make the present section, or rather Ref. 10, self-contained we introduce the concept in physical terms. For mathematical details the reader is referred to the original literature by J. Rappaz (references in Ref. 10).

In the presence of continua, i.e., in the presence of singularities, the numerical scheme should be able to model the physics near the singularity "precisely". If, for instance, we decided to model our cylindrical wave problem by ideal MHD, we would start with the equation of motion of MHD

$$-\omega^2 \rho_0 \vec{\xi} = \vec{F}(\vec{\xi}) . \tag{5.15}$$

Here $\vec{\xi}$ is the fluid displacement and $\vec{F}$ the force acting upon a fluid element. After constructing the variational form, which turns out to be a strong form, we would naively discretize the 3 components ξ_r, ξ_θ and ξ_z with the ansatz (5.11), and then solve the resulting discretized eigenvalue problem,

$$-\omega^2 A_{ij} x_j = B_{ij} x_j , \quad i = 1, \ldots, "3n" . \tag{5.16}$$

We would be punished for our naivity by solutions with spurious eigenfrequencies which have nothing to do with the fast nor the slow magnetosonic wave nor would they satisfy $A = \omega^2/v_A^2 - k_\parallel^2 = 0$ somewhere inside the plasma. This phenomenon is known as "spectral pollution". The reason for it is that in MHD the Alfvén waves are characterized by $\operatorname{div} \vec{\xi} = 0$ which cannot be satisfied other than pointwise with the ansatz (5.11) for all components of ξ. Phrased otherwise, the numerical scheme is unable to model the disparate singularities of $\xi_r \sim \log(r-r_0)$ and of ξ_θ, $\xi_z \sim 1/(r-r_0)$.

The remedy to pollution, once it is found, is obvious. Either one writes the equations in variables which have all the same type of singularity (e.g. eqs (3.34) and (3.35), $E_\perp \sim B_\parallel \sim \log(r-r_0)$) or one tackles directly the second order equation (3.37), or, as in the case of the eigenvalue problem where these two former approaches are unpractical one chooses a functional space of approximating functions which allows div $\vec{\xi} = 0$ everywhere. Inspecting

$$\operatorname{div} \vec{\xi} = \frac{\partial \xi_r}{\partial r} + \frac{1}{r}\left(\xi_r + im\,\xi_\theta\right) + ik\,\xi_z \tag{5.17}$$

one finds that ξ_r should be approximated according to eq. (5.11), the variables $\xi_2 = (\xi_r + im\ \xi_\theta)/r$ and ξ_z, however, by piecewise constant functions $\phi_{i+1/2}(x)$:

$$\begin{aligned}
\xi_r &= \sum_{i=0}^{n} x_i^{(r)}\, \psi_i(r) \ , \\
\xi_2 &= \sum_{i=0}^{n-1} x_{i+\frac{1}{2}}^{(2)}\, \phi_{i+\frac{1}{2}}(r) \ , \\
\xi_z &= \sum_{i=0}^{n-1} x_{i+\frac{1}{2}}^{(z)}\, \phi_{i+\frac{1}{2}}(r) \ ,
\end{aligned} \tag{5.18}$$

where

$$\phi_{i+\frac{1}{2}}(r) = \begin{cases} 0 & r < r_i \ , \ r > r_{i+1} \\ 1 & r_i \le r \le r_{i+1} \end{cases} \ . \tag{5.19}$$

This procedure yields a pollution-free spectrum. This is another point for our rule of thumb that the simplest possible approximation should be used.

6. APPLICATIONS

The aim of these lectures has been to introduce the main underlying ideas of the theory, or maybe rather of our computations, concerning AWH. If we now browse through our published work it should be possible to achieve a good understanding of the mainly numerical results. We shall chronologically go through this literature. It is natural that the earlier papers offer a less-clear physical picture than the more recent ones. The earlier papers contain nevertheless some not-unimportant results.

6.1 Ideal-MHD theory

6.1.1 Cylinder geometry

In the earliest conference papers [36,37] mainly the performance-tests of the numerical scheme have been reported. At that time the relation between mesh size and artificial damping ν became clear. Also we found that it should be possible to heat the interior of a cylindrical plasma, in contrast to the prediction made with simple models. Subsequently we found [38] that the resonance with the surface mode (which was called "a collective mode" at that time) was responsible for the good absorption in the plasma interior and an antenna optimization has been presented.

The role of cylindrical geometry (in contrast to plane slab geometry) has then been evidenced [21]. We have shown that the fact that the two geometries lead to different types of singularities must be related to the other fact, namely, that the energy does not penetrate to the center in the plane geometry. With the present knowledge we can say even a bit more. In ideal MHD, i.e., $\omega_{ci} \to \infty$, the quantity G, eq. (3.32), is non-zero merely due to the equilibrium current term. In Ref. 21 we called this term a "curvature term" because in plane geometry the equilibrium current does not generate a $G \neq 0$. To excite a singular Alfvén motion near the axis we rely on $G \neq 0$, eq. (3.51), because for the driving surface mode, S, $B_{\parallel} \to 0$ near the axis, Fig. 4.6.

The next paper [27] is a kind of review of the numerical results concerning resonant absorption. Poloidal antennae with feeders are introduced for the first time and we compare them with helical ones. We find a ratio of the antenna-loading resistances consistent with eq. (4.25). In a didactical part we show how the plasma perturbation evolves in time and numerical evidence for the collective plasma motion at the frequency of the surface mode is given. Then the limits to the computational model are described in detail showing results from a time-evolution code based on the MHD equation of motion, eq. (5.15),

$$\rho_0 \, \partial^2 \vec{\xi} / \partial t^2 = \vec{F}(\vec{\xi}) , \qquad (6.1)$$

and from an "artificially-damped" code. The antenna optimization studies are completed by considering the influence of the conducting shell and some preliminary results ($\omega/\omega_{ci} = 0$!) are presented on the antenna-plasma coupling via higher radial eigenmodes of the fast magnetosonic wave. As we would expect from Fig. 4.4 it is difficult to couple energy to the plasma interior in this way. A further result is that "very-low frequency heating", i.e., AWH with parameters such that $k_\parallel(r_o) \approx 0$, has low efficiency ($P/A \sim k_\parallel^3$).

Apart from the idea that the global eigenmodes of the Alfvén wave (GEAW) could be excited for the purpose of heating, the last two papers in this series [33,39] are of possibly mere historical interest. We show in fact that the ion-cyclotron waves, i.e., the global eigenmodes of the Alfvén wave, do exist even in MHD where $\omega/\omega_{ci} = 0$. Their existence is due to the "curvature"-term, $G \neq 0$. In MHD their distance (in frequency space) from the lower edge of the continuum is sizable only for very special choices of k. This distance can be strongly modified by finite-ω/ω_{ci} effects which, therefore, should be included into the model.

6.1.1 Toroidal geometry

In the paper just described [39] it is mentioned that the GEAW's can also be obtained in toroidal geometry but that it is not easy to model them. The problem is a mesh-resolution problem because the GEAW's are very densely packed in frequency. Since a given spatial mesh size requires a damping ν of a given size in order to make the numerical

continuum look as real continuum, GEAW's at a distance $\Delta\omega$ from the continuum disappear in the continuum if $\Delta\omega < \nu$.

In the two papers entirely devoted to toroidal geometry [9,40] only the physics relevant to resonant absorption is investigated. Reference 9 contains preliminary physical results and a part on numerics. We show that the mesh size and the damping ν in our toroidal code are sufficiently small to make the antenna-loading impedance P/A independent of ν. More details on the numerical features are given in Ref. 41 which is the preprint of Ref. 40.

The main physical results are given in Ref. 40. The formulation of the theory in toroidal geometry closely parallels that of ideal-MHD stability. The numerical code used is, in fact, a slightly modified version of the Lausanne MHD-stability code ERATO [42]. The main new feature in an axisymmetric configuration, as opposed to a cylindrically-symmetric configuration, is the phenomenon of poloidal-mode coupling. The poloidal wavenumber m ceases to be a good "quantum number". Even in a torus with circular cross-section the (1/R)-dependence of the toroidal magnetic field, B_T, breaks the circular symmetry : the equilibrium quantities, in particular B_T, depend on the poloidal angle. A rough approximation of the toroidal field is

$$B_T(r,\theta) = B_T(r=0) \Big/ \left(1 + \frac{r}{R_0}\cos\theta\right), \qquad (6.2)$$

where $B_T(0)$ is the value of the field on the magnetic axis which has a major radius R_0, whereas r and θ are the minor-radius and the poloidal-angle coordinates, respectively. This dependence of B_T introduces a "toroidal coupling" between modes of wavenumber m and wavenumber $m \pm 1$. The strength of the coupling is proportional to r/R_0. Clear numerical evidence for this coupling is shown. An antenna with single helicity (k,m) excites resonant surfaces with different m-numbers on different minor radii. Despite of the toroidal coupling the torus still behaves similarly to a cylinder. The resonance with the surface mode is still present.

Non-circular cross-sections introduce other types of linear mode coupling. An elliptical cross-section leads to coupling between m and $m \pm 2$ modes, triangularity couples m and $m \pm 3$ and so forth. Elliptici-

ty is discussed in detail and it is shown that an elliptical cross-section might be a problem for AWH because a substantial amount of energy can be coupled into resonant surfaces near the plasma boundary. This finding is confirmed by an investigation of a JET-like equilibrium.

From cylindrical antenna-optimisation studies [38] we had found that for m = 1 one should use $kr_p \approx 1.5\text{-}2$, corresponding to a toroidal wavenumber of the order of n = 4-6. The toroidal calculations made the optimum somewhat questionable. It is not that we would not find the highest P/A values in the range n = 4-6 but high n-numbers imply the existence of many resonant surfaces in the plasma and of some of them near the edge. We can avoid edge coupling by using small n, say n = 1-2. The price we have to pay is a somewhat smaller antenna load P/A.

6.2 Cold-plasma model

By "cold-plasma" model we mean the model developped in chapter 3. In the first paper using this model [17] we study the influence of the value of ω/ω_{ci} on the antenna load when the surface mode S or the fast magnetosonics modes $F_1^{m=1}$ and $F_2^{m=\pm 1}$ are excited. We find that the surface mode has the best penetration properties. Also we show that the distance of the GEAW from the continuum increases for increasing ω/ω_{ci}. This was an important fact which allowed us to explain experimental findings [44]. The next paper [29] is devoted to the spectra of a cylindrical column. Its first part, namely the one concerning a homogeneous cylinder, has been integrated into these lecture-notes (sect. 4.6). In the remaining part we show how these spectra are modified by inhomogeneities. In a recent conference paper [34] we then show the complications which might arise in a two-species plasma with two continua and two ω_{ci}-lines. The results of this paper based on cylindrical geometry should, however, not be over-valued because the physics near ω_{ci} is intrinsically toroidal.

In another very recent paper [24] we have made an effort to model AWH in a plane slab geometry. This paper has been commented in section 3.2.3.

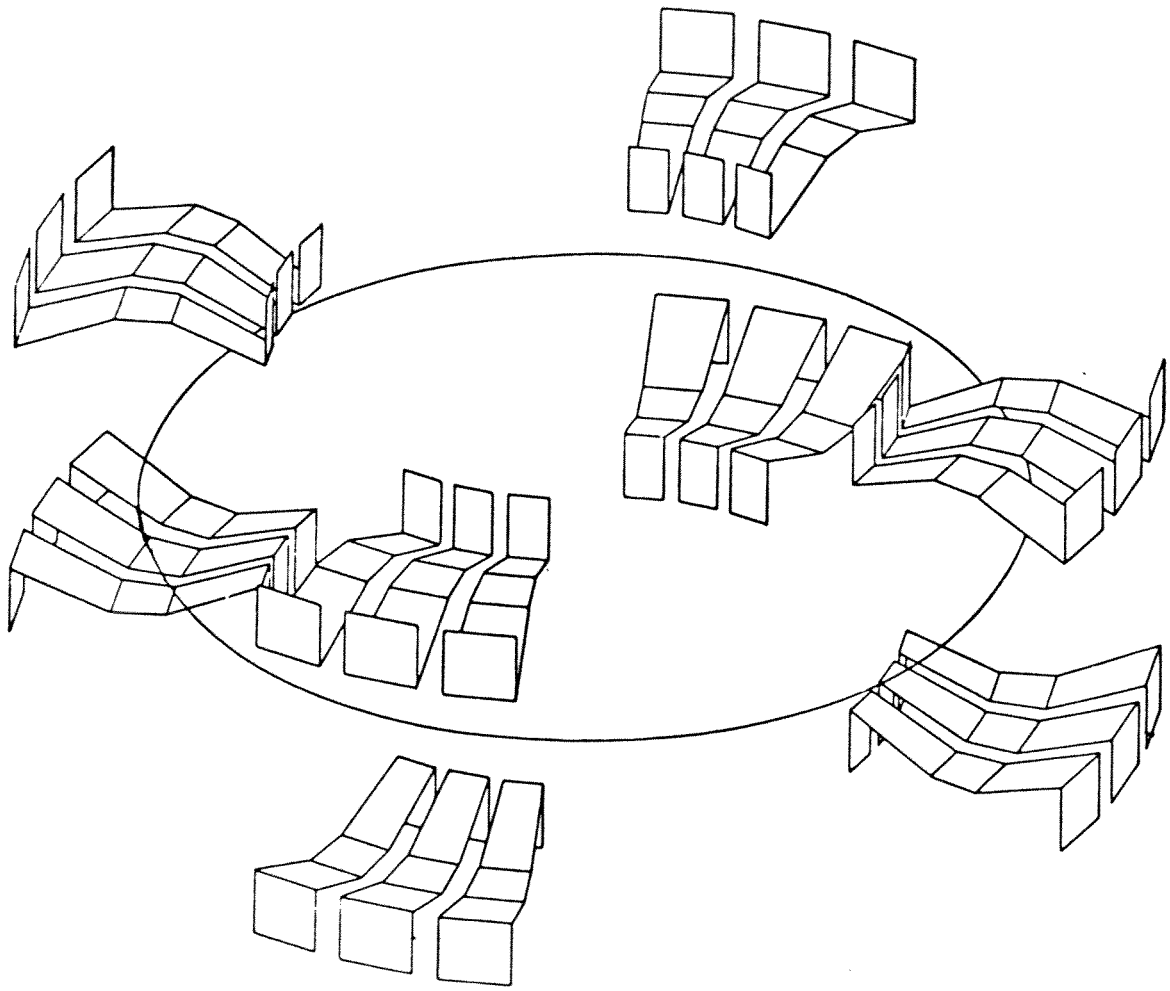

Fig. 6.1

6.3 Comparison with the TCA-experiment

6.3.1 Apparent resistance of the antenna

For a comparison the real antenna structure used in TCA has to be taken into account, Fig. 6.1, or at least certain features of it. The structure comprises eight separate antenna groups sited above and below the plasma at four equally spaced toroidal locations. Each group is fed separately with its phase determined by its external circuitry. Depending on relative phase, different excitation patterns can be achieved. With equal phase in the top- and bottom groups one has an "M=0 pattern", a phase of π makes it into a "M=1 pattern". In the toroidal direction there are 3 possibilities : equal phase yields N=0, two subsequent groups with equal phase and a phase of π in between the 2 pairs yield N=1, and the most commonly used pattern, N=2, is obtained by alterating the phase from group to group. Three examples of phasing are shown in Fig. 6.2.

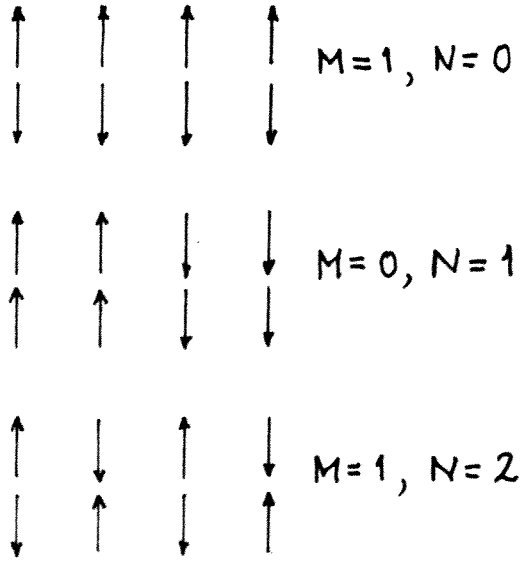

Fig. 6.2

The antennae cover a substantial fraction of the total toroidal surface. One group of three antenna plates covers a poloidal and a toroidal angle of 95 deg and 26 deg, respectively. The beneficial consequence of these wide angles is that the modes with high n or m are weakly excited.

Our theoretical model for an antenna consists of an imposed current in the vacuum. In the model the antennae cannot react to plasma motions by carrying image currents as the real metallic antenna plates can. In the experiment the effect of image currents is lowered by the fact that each antenna group is made up from 3 separate plates.

Any of the mentioned antenna patterns can be Fourier-analysed in terms of standing waves of the type $A_{mn}\ \cos m\theta\ \sin n\phi\ \sin\omega t$ (cylindrical approximation). Here $n = kR_o$, where R_o is the major radius. The M=0 and M=1 patterns engender m=0,2,4,... and m=1,3,5,... The toroidal patterns N=0,1,2 yield n=0,4,8,..., n=1,3,5,... and n=2,6,8,... respectively. The amplitudes A_{mn} corresponding to n=N and m=M are usually dominant.

Let us define the apparent series resistance of the antenna structure by

$$P = \frac{1}{2} R I^2, \tag{6.3}$$

where P is the total absorbed power, theoretically given by eq. (4.18), and I is the amplitude of the antenna current in one group. We can obtain a theoretical value for P. First, we have to Fourier-analyse the structure as described. Then, we have to decompose the standing waves into the 4 running waves of the types $(m\theta+n\phi-\omega t)$, $(m\theta-n\phi-\omega t)$, $(-m\theta+n\phi-\omega t)$ and $(-m\theta-n\phi-\omega t)$ compatible with the theory which treats a dependence $\exp[i(m\theta+n\phi-\omega t)]$. Knowing the amplitudes of the poloidal current, j_θ, eq. (4.4), of each of these modes we know the corresponding β and can calculate the power P from P/A, eq. (4.20), for each mode separately. Finally, the powers can be summed and multiplied by $2/I^2$ to obtain the resistance. Note that the eq. (4.20) should be used with s=1, characterizing a poloidal antenna with radial feeders. The radial currents need not to be Fourier-analysed separately, their Fourier-decomposition being automatically determined by div $\vec{j}$=0. A typical value obtained for TCA-parameters and M=1, N=2 is R=1Ω.

6.3.2 Rough general scaling

Most of the global physical parameters can be scaled out of the theory, sect. 4.5. The same is true for the experimental results within certain limits [14]. A plot of R/ω [mΩ/MHz] versus normalized frequency $\underset{\sim}{\omega}=\omega r_p/v_A(0)$ for different parameters (B_T,ω) shows that these are scaled out. The resistance has the theoretical scaling, $R=(v_A(0)/c^2)\,\underset{\sim}{R}$. If we argue that the loading is due to AWH we might replace $\underset{\sim}{\omega}$ by $\underset{\sim}{k}_\parallel$ and R/ω by $r_p\,\underset{\sim}{R}/(c^2\underset{\sim}{k}_\parallel)$ and find, indeed, that R/ω should depend on $\underset{\sim}{k}_\parallel$ as $\underset{\sim}{R}(\underset{\sim}{k}_\parallel)/\underset{\sim}{k}_\parallel$. Effects of a finite value of ω/ω_{ci} were not considered in this scaling.

6.3.3 Resistance traces

In the early low-power measurements (~100 W) the density was usually ramped which is equivalent to a monotonic increase of $\underset{\sim}{\omega} = \omega r_p/v_A(0)$. In this way a large frequency band of the spectrum is probed by the driver. The experiments showed a loading in the continuum which was quite consistent with MHD calculations. The peaks due to the global eigenmodes of the Alfvén wave (GEAW), however, came unexpected. Although they have subsequently been explained by means of the MHD model, good agreement could only be obtained by including the effects of ω/ω_{ci} [17,43].

Consistent with theory the GEAW's appear only with a helicity having the same sign as that of the equilibrium magnetic field. Their wave form, inferable from sawtooth oscillations on magnetic probes and on soft x-ray signals [15], seems also to be consistent with theory. The distance between subsequent GEAW's [44] can be explained with the finite-ω/ω_{ci} model.

6.3.4 High-power experiments [45,46]

To date peak powers up to 220 kW and average powers (30 msec) up to 170 kW have been injected into TCA. These powers are of the order of the ohmic heating power before the RF pulse is applied. No manifestly nonlinear effect related directly to the heating scheme has been observed. There is, however, an impurity problem and, in general, the elec-

tron density increases substantially during the RF pulse. These two phenomena have a remarkable similarity with what is known from ICRF experiments. Both, the ion and the electron temperature increase at the beginning of the RF-pulse. The increase is roughly linear with the delivered power. Towards the end of the pulse the electron temperature decreases due to the radiated power loss caused by the impurities. The ion temperature increases throughout the RF-pulse.

7. OUTLOOK TO ICRF

As several times mentioned, the ICRF mode-conversion scenario has much in common with AWH. There is, however, one essential difference : ICRF cannot be modelled in cylindrical geometry because the lines $\omega=\omega_{ci}$ are vertical lines through the plasma cross-section, which spoil what remains of the "cylinder" in a torus. The theoretical tools in the past applied to ICRF have been the WKB-method in all kinds of geometries and the "full bounded-wave concept" restricted to plane-slab or belt geometry. By "full bounded-wave concept" we mean the approach described in these notes.

It is only now that attempts are made [47,48] to tackle the toroidal ICRF-problem in this way. A possible path to reach the goal is evident from these notes. The basic wave equation, eq. (3.28), has to be written in toroidal magnetic coordinates in the same way as we have done it for the cylinder. The resulting equations have much in common with the ideal-MHD equations. The difficult part, namely the operator rotrot is the same as in MHD. The modification of ERATO [42] is in progress. This and the previously-mentioned codes [47,48] should be useful to assess the limitations of the ray-tracing codes based on the WKB-method and applicable to large-size devices; they should be useful to model ICRF on medium-size devices, and last but not least, should decide on the question whether or not the resonant surfaces of ICRF coincide with magnetic surfaces as it is the case in AWH for $\omega/\omega_{ci}=0$. There are, in fact, strong analytical indications [49] which say that the surfaces indeed do coincide.

8. ACKNOWLEDGEMENTS

The authors wish to acknowledge useful discussions with B.E. Clancy, R. Gruber and A. Pochelon. They are indebted to Prof. King Hay Tsui without whose interest into Alfvén Wave Heating this report would no have been written.

One of the authors (K.A.) thanks Prof. King Hay Tsui for the kind invitation to the Universidade Federal Fluminense (UFF) and for his most generous hospitality. He is grateful to all the members of the plasma physics group of UFF for the warm reception. He also would like to thank the Financiadora de Estudos e Projetos (FINEP) for the local living expenses through the Convenio FINEP/UFF-Pesquisas em Física de Plasmas, and the Conselho Nacional de Desenvolvimento Científico e Tecnológico (CNPq. Auxilio, Processo no. 40.5462/83-FA) for the kind offer of the air ticket.

This work has been supported by the Ecole Polytechnique Fédérale de Lausanne, by the Swiss National Science Foundation and by Euratom.

9. REFERENCES

[1] A. Hasegawa and L. Chen, Phys. Rev. Lett. 35 (1975) 370; Phys. Fluids 19 (1976) 1924

[2] D.W. Ross, G.L. Chen, and S.M. Mahajan, Phys. Fluids 25 (1982) 652

[3] V.L. Ginzburg, "The propagation of electromagnetic waves in plasmas", Pergamon, Oxford, 1970

[4] T. Speziale and P.J. Catto, Phys. Fluids 20 (1977) 990 and papers cited therein.

[5] L.A. Artsimowitsch und R.S. Sagdejew, "Plasmaphysik für Physiker" (in German), Teubner, Stuttgart, 1983

[6] A. Hasegawa and L. Chen, Phys. Rev. Lett. 23 (1974) 454; Phys. Fluids 17 (1974) 1399

[7] M. Abramowitz and I.A. Stegun, "Handbook of mathematical functions", Dover, New York, 1964, 1970

[8] E.T. Whittaker and G.N. Watson, "A course of modern analysis", Cambridge University Press, 1927

[9] K. Appert et al., Proc. Heating in Toroidal Plasmas, Como 1980, Commission of the European Communities, Bruxelles 1981, vol. II, p. 643

[10] K. Appert et al., Comput. Phys. Commun. 24 (1981) 329

[11] J. Tataronis and W. Grossmann, Z. Physik 261 (1973) 203 and 217

[12] E.M. Barston, Annals Phys. 29 (1964) 282

[13] Z. Sedlacek, J. Plasma Phys. 5 (1971) 239, ibid. 6 (1971) 187 and Czech. J. Phys. B23 (1973) 892

[14] A. de Chambrier et al., Plasma Phys. 24 (1982) 893

[15] A. de Chambrier et al., Phys. Lett. 92A (1982) 279

[16] R.D. Bengston et al., Proc. Heating in Toroidal Plasmas, Grenoble 1982, Commission of the European Communities, Bruxelles 1982, vol. I, p. 151

[17] K. Appert and J. Vaclavik, Plasma Phys. 25 (1983) 551

[18] T.H. Stix, "The theory of plasma waves", McGraw-Hill, New York, 1962

[19] K. Appert, R. Gruber, and J. Vaclavik, Phys. Fluids 17 (1974) 1471

[20] C.F.F. Karney, F.W. Perkins, and Y.-C. Sun, Phys. Rev. Lett. 42 (1979) 1621

[21] K. Appert, B. Balet, and J. Vaclavik, Phys. Lett. 87A (1982) 233

[22] T.H. Stix and G.W. Swanson, Princeton Report, PPPL-1903, June 1982, prepared for "Handbook of Plasma Physics", vol. I, A. Galeev and R.N. Sudan editors, NHPC, Amsterdam

[23] A. Pochelon et al., Proc. 7th Europ. Conf. on Contr. Fusion and Plas. Phys., Lausanne, 1975, vol. I, p. 157; R. Keller, Lausanne Report LRP 104/76

[24] S. Succi et al., Helv. Phys. Acta 57 (1984) 121

[25] M. Cotsaftis and W.N-C. Sy, Phys. Lett. 93A (1983) 193

[26] V.D. Shafranov, Sov. Phys. Tech. Phys. 15 (1970) 175

[27] B. Balet, K. Appert, and J. Vaclavik, Plasma Phys. 24 (1982) 1005

[28] S. Ichimaru, "Basic Principles of Plasma Physics", Benjamin Inc., Reading (Mass.) 1973

[29] K. Appert, J. Vaclavik, and L. Villard, Phys. Fluids 27 (1984) 432

[30] M.S. Chance et al., Nucl. Fusion 17 (1977) 65

[31] L.J. Lanzerotti et al., Phys. Rev. Lett. 31 (1973) 624

[32] F. Paoloni, Phys. Fluids 18 (1975) 640

[33] K. Appert et al., Proc. Heating in Toroidal Plasmas, Grenoble 1982, Commission of the European Communities, Bruxelles 1982, vol. I, p. 203

[34] K. Appert, J. Vaclavik, and L. Villard, Proc. 11th Europ. Conf. on Contr. Fusion and Plas. Phys., Aachen 1983, Part I, p. 305 in Europ. Conf. Abstracts, vol. 7D

[35] G. Strang and G.J. Fix, "An analysis of the finite element method", Prentice-Hall, Englewood Cliffs, 1973

[36] B. Balet et al., ZAMP 30 (1979) 845

[37] B. Balet et al., Proc. 9th Europ. Conf. on Contr. Fusion and Plas. Phys., Oxford 1979, vol. I, p. 170

[38] K. Appert et al., Plasma Physics and Contr. Nucl. Fusion Research 1980 (Proc. 8th Int. Conf., Brussels, 1980), vol. 2, IAEA, Vienna (1981) p. 43

[39] K. Appert et al., Plasma Phys. 29 (1982) 1147

[40] K. Appert et al., Nucl. Fusion 22 (1982) 903

[41] K. Appert et al., Lausanne Report, LRP 187/81, 1981

[42] R. Gruber et al., Comput. Phys. Commun. 21 (1981) 323; ibid. 24 (1981) 363

[43] K. Appert et al., Proc. 11th Europ. Conf. on Contr. Fusion and Plas. Phys., Aachen 1983, Part I, p. 301 in Europ. Conf. Abstracts, vol. 7D

[44] A. de Chambrier et al., Proc. Heating in Toroidal Plasmas, Grenoble 1982, Commission of the European Communities, Bruxelles 1982, vol. I, p. 161

[45] A. de Chambrier et al., Plasma Physics and Contr. Nucl. Fusion Research, 1982 (Proc. 9th Int. Conf., Baltimore, 1982), paper J-1-1 and Plasma Phys. 25 (1983) 1021

[46] R. Behn et al., Plasma Physics and Contr. Fusion 26, vol. 1A (1984) 173 (Proc. 11th Europ. Conf., Aachen, 1983)

[47] D.Q. Hwang, private communication, Paris, Nov. 1983; P.L. Colestok and R.F. Kluge, Bull. APS, Part II, 27, No. 8 (1982) 1076

[48] K. Itoh, S.-F. Itoh, and A. Fukuyama, Nuclear Fusion 24 (1984) 13

[49] T. Hellsten and E. Tennfors, Proc. 9th Europ. Conf. on Contr. Fusion and Plas. Physics, Oxford 1979, vol. I, p. 15